www.sciencemag.org/cgi/content/full/science.aaa2773/DC1

Supplementary Materials for

The makers of the Protoaurignacian and implications for Neandertal extinction

S. Benazzi,* V. Slon, S. Talamo, F. Negrino, M. Peresani, S. E. Bailey, S. Sawyer, D. Panetta, G. Vicino, E. Starnini, M. A. Mannino, P. A. Salvadori, M. Meyer, S. Pääbo, J.-J. Hublin

*Corresponding author. E-mail: stefano.benazzi@unibo.it

Published 23 April 2015 on *Science* Express
DOI: 10.1126/science.aaa2773

This PDF file includes:

- Materials and Methods
- Supplementary Text
- Figs. S1 to S11
- Tables S1 to S10
- References (*37*–*127*)

Materials and Methods

Morphometric analysis

3D enamel thickness

To quantify the 3D enamel thickness, high-resolution micro-CT images of Bombrini, as well as 18 recent modern human (RMH) deciduous lower second incisors (Northern Italian Medieval and Renaissance specimens housed at the Department of Cultural Heritage, Ravenna, University of Bologna, Italy) were obtained with the Xalt micro-CT scanner *(37)* (Institute of Clinical Physiology, National Research Council, Pisa, Italy). All teeth were scanned at 50 kVp, 2 mm Al filtration, 960 views over 360°, 1.6 mAs/view. All the images were reconstructed using a modified Feldkamp-type cone beam Filtered Backprojection (FBP) algorithm *(38)* with embedded compensation of mechanical misalignments. The isotropic voxel size of 18.4 μm^3 on a 512x512x1200 volume dataset and then cropped to the tightest bounding box of each tooth. The micro-CT images were segmented in MeVisLab 2.4 (MeVis Medical Solutions AG, Bremen, Germany) using a global threshold calculated as the mid-value (in Hounsfield Units) between the dentin and enamel peaks in the image stack histogram. The segmented enamel cap and virtually filled dentin were then converted to meshes using the Winged-Edge Mesh (WEM) tool and exported in Standard Tessellation Language (STL) file format for subsequent analysis.

Additional comparative data for five Neandertals (Abri Suard, Amud 7, Kebara 1, La Ferrassie 8, Roc-de-Marsal 1) were obtained with a BIR SN001 microtomographic system (Max Planck Institute for Evolutionary Anthropology, Leipzig, Germany) using the following scan parameters: 130 kV, 100 µA, with a brass filter of 0.25 mm (for Abri Suard and Roc de Marsal 1) and 0.50 mm (for Kebara 1 and Amud 7) thickness; 100 kV, 200 µA, with a brass filter of 0.25 mm for La Ferrassie 8. Volume data were reconstructed using isometric voxels ranging between 16.41 µm and 36.44 µm. The micro-CT images of the Neandertal sample were virtually segmented using a semiautomatic threshold-based approach in Avizo 7 (Visualization Sciences Group Inc.) to reconstruct 3D digital models of the teeth.The digital models were then imported in Rapidform XOR2 (INUS Technology, Inc., Seoul, Korea). Following indications provided by Benazzi and colleagues *(17)*, the entire enamel cap was considered, while the coronal dentine was separated from the root dentine using a spline curve digitized along the cervical line. This curve was interpolated with a smooth surface to seal the bottom of the dentine core.

We measured the volume of the enamel cap (mm^3); the volume of the dentine core (which includes the volume of the coronal pulp - mm^3); the enamel-dentine junction (EDJ) surface (the interface between the enamel cap and the dentine core - mm^2). These measurements were used for the computation of both the 3D average enamel thickness (3D AET = volume of enamel divided by the EDJ surface; index in millimeters) and the 3D relative enamel thickness index (3D RET = the average enamel thickness index divided by the cubic root of dentine volume; scale free index) (Table S2). Standardized scores (Z-scores) of Bombrini crown BL diameters and RET index were computed to establish to which group means the value of Bombrini was closest to.

Digital simulations of tooth wear and mesial damaging

Since Bombrini is rather worn and the enamel is chipped off mesially, two RHS specimens (Guid_T39 and Sgvald_T59) were digitally worn down and mesially damaged simulating a condition comparable to Bombrini to evaluate whether the loss of enamel on the mesial side of the Bombrini tooth affects the computed AET and RET indices, and ultimately its taxonomic attribution. Since Ungar and colleagues *(39)* did not find any clear pattern of beveling with tooth wear in permanent lower incisors, we defined an objective procedure to digitally wear and damage the two RHS specimens that involves the following steps (Fig. S8): the best-fit plane through the points of the incisal surface (incisal plane) of Bombrini was computed (Fig. S8A); the crown of the two RHS specimens was superimposed to the crown of Bombrini using Iterative Closest Point, an algorithm that minimizes the distance between two point clouds by the least squares method *(40)* (Fig. S8B), and the portion of crown above the incisal plane was removed (Fig. S8C); for both RHS specimens, the portion of enamel in correspondence to the Bombrini's mesial damage was removed (Fig. S8C), whereas the underlying dentine was preserved (Fig. S8D), and the 3D enamel thickness was computed (Table S3).

Ancient DNA

DNA extraction and library preparation

Following the removal of surface material, two samples, of 20mg and 17mg, were removed from the root of the Fumane 2 tooth using a sterile dentistry drill. DNA was extracted from each sample as described *(41)* and eluted in TE (10mM Tris-HCl, 1mM EDTA, pH 8.0). Three libraries (A4678, L9358 and A4679) were prepared using 5µl, 10µl and 15µl of the first DNA extract (E1119), respectively. Two libraries (L5184 and L5185) were prepared using 15µl of the second DNA extract (E2748). All libraries were created using a single-stranded DNA library preparation protocol *(42).* Library L9358 was pre-treated with USER (New England Biolabs), a mixture of uracil DNA glycosylase (UDG) and endonuclease VIII, which removes uracil bases from the interior of DNA molecules and cleaves the DNA strands *(43, 44)*. All other libraries were not treated with USER, in order to maintain the complete cytosine (C) to thymine (T) substitutions signal. The number of DNA molecules in each library was determined by digital droplet PCR (BioRad QX 200), using 1µl of a 2,000-fold, 4,000-fold or 8,000-fold dilution of the library (for libraries L5184-L5185, A4678-A4679 and L9358, respectively) as template for an EvaGreen (BioRad) assay with primers IS7 and IS8 *(45)*. Each library was tagged with a pair of unique indexes *(46)* and amplified using AccuPrime Pfx DNA polymerase (Life Technologies) *(47)*. Amplification products were purified using the MinElute PCR purification kit (Qiagen).

Mitochondrial capture and sequencing

0.6µg of library L9358 was enriched for human mtDNA once, as described *(48)*. 1µg of libraries L5184, L5185, A4678 and A4679 was enriched as described *(49)*. A second round of mitochondrial enrichment was performed for libraries A4678 and A4679, using

0.5µg of input DNA. The enriched libraries were sequenced on Illumina's MiSeq platform using two paired-end runs (2x 76 cycles) with double-index configuration *(46)*.

Raw sequence processing and mapping

Base calling was performed using IBIS *(50)* for library L9358 and using Bustard (Illumina) for all other libraries. Only sequences which perfectly matched the expected index combinations were retained. Adapter sequences were trimmed, and forward and reverse reads were merged into a single sequence *(51)*. Merged sequences were aligned to the revised Cambridge Reference Sequence (NC_012920), using BWA *(52)* with the parameters "-n 0.01 -o 2 -l 16500", i.e., with seeding turned off and allowing for more mismatches and gaps than default parameters *(44)*. PCR duplicates were removed by calling a consensus from sequences with identical alignment start and end coordinates using bam-rmdup (https://github.com/udo-stenzel/biohazard). Only sequences longer than 35 bases and with a mapping quality greater than 30 were retained for further analyses.

Phylogenetic inferences

Libraries prepared from the first DNA extract of the Fumane 2 specimen (A4678, A4679 and L9358) yielded too few informative mtDNA sequences to reconstruct a complete mtDNA genome (Table S4). We nonetheless investigated the phylogenetic position of the Fumane 2 mtDNA sequences recovered in these libraries, using two sets of 'diagnostic' sites. The first set is composed of 63 positions at which modern humans (n=311) *(20)* differ from all ten Neandertals for which complete mtDNA genomes have been sequenced *(20, 54-58)*. The second set is composed of 17 positions at which modern human mitochondrial genomes (n=311) differ from the Neandertal (n=10), Denisovan (n=3) and chimpanzee (*Pan troglodytes*) (n=1) genomes. We used these sites to determine whether overlapping sequences carry the human or the Neandertal state, once using all mapped sequences at least 35bp in length and once using only sequences with a C to T difference to the reference genome at the 5' and/or 3' terminal position.

The two libraries rich in mitochondrial sequences (L5184 and L5185) were merged using SAMtools (https://github.com/samtools/samtools). The mitochondrial genome was reconstructed using an in-house PERL script. A consensus base was called only at positions covered by a minimum of 5 sequences, at least 80% of which presented an identical base. This analysis was carried out once using all sequences, and once using only sequences carrying a C to T substitution at a terminal position. For the latter, prior to calling a consensus base, any terminal T at a position where the reference base is a C was converted to an N, to prevent damage-induced C to T substitutions from affecting the downstream phylogenetic analyses.

The reconstructed mitochondrial genome from Fumane 2 was aligned to the mtDNA sequences of 54 present-day humans from a variety of geographical origins *(53)*, 10 ancient modern humans *(25, 26)*, 10 Neandertals *(20, 54-58)*, 2 Denisovans *(24, 59)*, a hominin from Sima de los Huesos *(55)* and a chimpanzee (NC_001643 *(60)*) using MAFFT *(61)*. The D-loop (positions 16024-576) was excluded, as it does not evolve at a constant rate across all human lineages *(53)*. A Neighbor-Joining tree was constructed using MEGA6 *(62)*. The support for the resulting phylogeny was tested by bootstrap resampling with 500 replications.

Polymorphic positions in the Fumane 2 mtDNA genomic sequence were determined by alignment to the revised Cambridge Reference Sequence. The mitochondrial haplogroup was assigned to the consensus genome sequence using Haplogrep (based on Phylotree build 16) *(63, 64)*.

Molecular dating

The number of mutations occurring on the Fumane 2 branch, since its split from the most recent common ancestor with another human mtDNA genome, was inferred by analysis of pairwise differences. The differences were evaluated compared to a present-day human from China (AF346972) and an ancient modern human (Ust-Ishim, PRJEB6622), using the mitochondrial genome of a present-day San individual (AF347008) as an outgroup. The difference in the number of mutations occurring on each branch was translated to differences in time, based on a mitochondrial mutation rate of $2.53*10^{-8}$ substitutions per site per year (95% highest posterior density [HPD]: $1.76\text{-}3.23*10^{-8}$) *(26)*.

Furthermore, we estimated the tip date of the Fumane 2 branch in a Bayesian framework using BEAST *(65)*, by aligning the Fumane 2 genome to 10 present-day humans and 10 directly carbon-dated ancient modern humans *(25, 26)*. The Hasegawa-Kishino-Yano model of nucleotide substitution, with a gamma-distributed rate of heterogeneity and a fixed proportion of invariant sites (HKY+G+I), was determined to be the best-fitting model using Modeltest 3.7 and PAUP* *(66)*. Models based on a strict molecular clock versus a log-normal uncorrelated relaxed clock were investigated, using a constant or a coalescent Bayesian skyline population size as priors. Based on the likelihood scores of the different models, we opted for a relaxed clock and a constant population size for the analysis. A Markov Chain Monte Carlo (MCMC) run with 30,000,000 iteration was run, sampling every 1,000 steps and discarding the first 6,000,000 iterations as burn-in.

Radiocarbon chronology

Sample selection and Method

In order to investigate the chronology of Palaeolithic sites, sample selection is the first aspect that should be considered. Bones with anthropogenic marks are the best samples to attest human presence at a site. However, this type of selection can have consequences for the quality of the collagen extracts *(3)*. In addition, the number of samples taken for radiocarbon dating is the second most important factor to be considered, in order to constrain the chronological events at the site.

At Riparo Bombrini, 32 samples were selected for radiocarbon dating; 29 animal bones (with and without anthropogenic marks) and three charcoal samples.

All 29 bone samples were pretreated at the Department of Human Evolution, Max Planck Institute for Evolutionary Anthropology (MPI-EVA), Leipzig, Germany, using the method described in Talamo and Richards *(67)*. The outer surface of the bone samples are first cleaned by a shot blaster and then 500mg of bone powder is taken. The samples are then decalcified in 0.5M HCl at room temperature until no CO_2 effervescence is observed, usually for about 4 hours. 0.1M NaOH is added for 30 minutes to remove humics. The NaOH step is followed by a final 0.5M HCl step for 15 minutes. The resulting solid is gelatinized following Longin *(68)* at pH3 in a heater block at 75°C for 20h. The gelatine is then filtered in an Eeze-Filter™ (Elkay Laboratory Products (UK) Ltd.) to remove small (<80 μm) particles. The gelatine is then ultrafiltered with Sartorius "Vivaspin Turbo" 30 KDa ultrafilters *(69)*. Prior to use, the filter is cleaned to remove carbon containing humectants *(70)*. The samples are lyophilized for 48 hours.

To verify the state of preservation of the collagen, the C:N ratio, %C, %N, collagen yield and $\delta^{13}C$ and $\delta^{15}N$ values must be evaluated. The C:N ratio should be between 2.9 and 3.6 and the collagen yield not less than 0.5% of weight *(71, 72)*. Stable isotopic analyses were undertaken at MPI-EVA, Leipzig (Lab Code S-EVA), using a Thermo Finnigan Flash EA coupled to a Delta V isotope ratio mass spectrometer.

The 13 bones that met the collagen quality criteria (Table S7) were sent to the Klaus-Tschira-AMS facility of the Curt-Engelhorn Centre in Mannheim, Germany (Lab Code MAMS), where they were graphitized and dated *(73)*. The three charcoal samples were sent directly to the Mannheim AMS laboratory, where they were pretreated with the ABOX method.

Chronological work at Riparo Bombrini

It should be pointed out that the G. Vicino excavation of 1976 was carried out through partially cemented sediments (as mentioned above in "*The discovery of the tooth"* paragraph), which were not affected by stratigraphic disturbances. On the other hand, some areas excavated in 2002-2005, located NW and SE of the 1976 trench, are probably problematic from a stratigraphic point of view. Here, soil forming processes affected the sequence in squares D1-F1 of the NW sector, outside the probable dripline of the former rock-shelter, and, consequently, the stratigraphy was difficult to read during fieldwork. However, the diagnostic lithic artefacts in these deposits were exclusively Protoaurignacian, suggesting that no major reworking occurred.

Pedogenesis was less developed within the inner part of the shelter, but disturbance may have been produced by the dumping of a large heap of waste exactly on top of the Bombrini deposits during the 19th century railway works or World War II destructions. However, it must be stressed that the site yielded only Protoaurignacian artefacts, and that no evidence of more recent cultural phases was identified in the shelter. If more recent levels existed, they were destroyed by the construction of the railway in 1870; in fact, very rare reworked Gravettian-Epigravettian tools were found only in the spoil heap of the railway construction works.
For these reasons we kept the two areas of excavation separate when we performed the Bayesian analysis. The radiocarbon results of Riparo Bombrini are listed in Table S7.

All dates were corrected for a residual preparation background estimated from pretreated ^{14}C free bone samples, kindly provided by the MAMS and pretreated in the same way as the archaeological samples.

All the samples were calibrated using IntCal13 *(29)* in the OxCal 4.2 program *(34)* (Fig. 3 and Fig. S11, Table S10). The t-type outlier analysis was performed to detect problematic samples, with prior probabilities set at 0.05. The results were linked with the (NGRIP) $\delta^{18}O$ climate record (*74, 75*).

Supplementary Text

Riparo Bombrini

Description of the site and history of the excavations

Riparo Bombrini is situated in an important archaeological area of shelters and caves known as Balzi Rossi (literally 'Red Rocks'), an impressive Jurassic dolomitic limestone cliff located on the Italian-French state border and facing the present-day seashore (Fig. S1). The name of the locality derives from the iron-rich minerals included in the limestone walls. The complex includes several caves and shelters, the most famous of which are Grotta dei Fanciulli, Riparo Lorenzi, Grotta di Florestano, Grotta del Caviglione, Barma Grande, Grotta del Bauso da Ture (now destroyed), Grotta del Principe, Grotta Costantini, Riparo Mochi and Riparo Bombrini (Fig. S2). Florestano I, Prince of Monaco, carried out the first archaeological research at Balzi Rossi in 1846-57. More recently, between 1928 and 1961, regular excavations were carried out by Alberto Carlo Blanc, Luigi Cardini, Paolo Graziosi and Aldobrandino Mochi, on behalf of the Italian Institute of Human Palaeontology *(76)*.

The richest series of Palaeolithic Venuses ever found in one place in Western Europe was discovered between 1883 and 1895 by Louis Alexandre Jullien at Barma Grande *(77)*; more recently, Upper Palaeolithic engravings and an incision representing a horse on the wall of Caviglione were also discovered *(78-80)*. Unfortunately, most of the caves were excavated by the first pioneers and explorers of the nineteenth century, and little or no stratigraphic information from these earlier excavations is available.

More recently, research was resumed: by the Musée d'Anthropologie Préhistorique de Monaco at Grotta del Principe, where a fossil fragment ascribed to *Homo heidelbergensis* was recovered in an Early Palaeolithic layer *(81)*; by Giuseppe Vicino at the site of the Ex-Casinò *(82, 83)*; by Mauro Cremaschi at the site of the Ex-Birreria *(84)* and by Amilcare Bietti and other scholars at Riparo Mochi *(8, 85-90)*.

Balzi Rossi is one of the most important prehistoric sites in Europe, because it preserves stratigraphic sequences that include layers with traces of Neandertal and anatomically modern human occupation. Here, the arrival of modern humans was much earlier than at other sites in Italy, as indicated by the radiocarbon dates for the Riparo Mochi sequence *(8)*. Moreover, several complete Gravettian burials have long been the focus of extensive anthropological research at international level *(91-93)*.

Riparo Bombrini is situated in a narrow area between the railway line connecting Genoa to Nice and an old storage-tank, not far from Grotta del Caviglione, where the engraving of the horse and the famous grave of the "Homme de Menton" (actually a woman) were found. The prehistoric sequence of this shelter was discovered by Émile Rivière during the second half of the XIX century *(94)*, but was excavated for the first time in 1938 by Luigi Cardini *(95)*. His small trench unearthed layers that can be ascribed to the Protoaurignacian. Cardini also found hearths, bones and abundant lithic artefacts, among which several characteristic Dufour bladelets. The shelter was explored again in 1976 by Giuseppe Vicino, during works for the construction of a pedestrian bridge that crosses over the railway and leads to the caves *(96)*. This new excavation explored an area 6 m^2 wide and about one metre deep. The human tooth analysed in this paper was discovered during these excavations *(97)*. Vicino unearthed a stratigraphic sequence formed by a thick layer with Protoaurignacian artefacts, overlying layers with Mousterian industries. Between 2002 and 2005, new archaeological excavations were carried out, with the goal of better understanding the Late Mousterian to Protoaurignacian transition. The rockshelter was excavated jointly by the Archaeological Superintendency of Liguria, the University of Pisa (Italy) and Duke University (North Carolina, USA), with the help of the Museo di Archeologia Ligure (Genova Pegli, Italy) and of the Istituto Internazionale di Studi Liguri (Bordighera, Italy). These last excavations were conducted next to the trench opened by G. Vicino, mainly focusing on Protoaurignacian layers, but also exploring Mousterian levels in a deep trench *(90, 98-103)*.

Stratigraphy

The stratigraphy presented here refers to the 1976 and 2002-2005 excavations (Fig. S3). The site was explored over an area of about 15 m^2. A trench approximately 10 m long, almost perpendicular to the wall of the former shelter, was excavated into the archaeological deposit to a maximum depth of 130 cm *(88, 99-101)*.

Some minor differences in the description of the stratigraphy occurred during the two campaigns.

The sequence was divided into four artificial spits by G. Vicino in 1976, who identified two cultural units: the lower one (Upper and Lower level IV) containing Mousterian material culture, the upper one (level III-I) containing Upper Palaeolithic artefacts. During the 2002-2005 excavations, these units were confirmed, but labelled differently. A description of the units identified during the latest field-work campaigns (2002-2005) and their correspondence with the levels defined by Vicino is reported here from the lowermost (oldest) to the uppermost (most recent):

- M7-M1: levels with abundant Mousterian industry, corresponding to “Lower level IV” of the 1976 excavation.
- MS2-MS1: levels with scanty evidence of Mousterian industry, corresponding to “Upper level IV” of the 1976 excavation.
- A3: it is the infill of a narrow channel with sub-cylindrical bottom, running along the wall of the shelter; it included calcareous rubble mixed with very few Protoaurignacian artefacts; charcoal useful for dating was absent. This level has no correspondence with the deposits explored by G. Vicino.
- A2: level with very abundant Protoaurignacian artefacts; it corresponds to “level III” of the 1976 excavation.
- A1: level with abundant Protoaurignacian artefacts, corresponding to “level II” of the 1976 excavation.
- Level I was identified only during the 1976 excavation and yielded several *Mytilus* sp. shells, possibly representing food refuse, but diagnostic artefacts were not present *(96)*.

Within the sequence, there is a sharp change between the lithostratigraphic units including Mousterian evidence and those with Protoaurignacian industry. The latest

Mousterian is included within units MS2 and MS1, characterised by large breakdown blocks suggesting a cold climate phase. The transition between these units and those above, containing Protoaurignacian artefacts, is marked by a clear discontinuity, which shapes the top of unit MS1 and testifies either a stop of sedimentation or an erosive phase. Levels A2 and A1 (respectively level III and II in 1976 excavation) are two artificial partitions of a single lithologic unit consisting of a yellowish silty-clay layer - probably a more or less altered loess - that includes abundant Protoaurignacian industry. Two superimposed hearths were found near the bottom wall of the shelter, respectively in levels A2 and A1; the lower one was situated inside a circular depression ("*en cuvette*") *(102)*.

The 1976 and 2002-2005 excavations yielded a very large quantity of knapped flint artefacts referable to the Protoaurignacian. Dufour bladelets are well represented, while formal tools and cores are scarce. Local raw material was mostly used, but exotic flint was also imported from France (Vaucluse, Estérel massif, various Provence outcrops) *(99, 102)*. Red radiolarite and *Scaglia rossa* flint are also present; the former comes from eastern Liguria and from the Parma area (Monte Lama-Catellaccio-Pràrbera), the latter from the Marche region, some 350 km away, on the Adriatic side of the Italian peninsula *(99, 104, 105)*.
Bone artefacts and personal ornaments such as perforated shells, steatite artefacts, engraved belemnites, worked bones, red ochre are also relatively common.

Fauna is well documented. It mainly comprises numerous small and often burnt bone fragments. Roe deer (*Capreolus capreolus*), chamois (*Rupicapra rupicapra*), and ibex (*Capra ibex*) are particularly abundant, indicating a relatively cold climate *(100)*.

The discovery context of the human tooth
The tooth was collected in 1976 by G. Vicino, while breaking a chunk of cemented sediment. It came from square B1, spit III-4, about 6 meters away from the shelter wall (Fig. S3, S4). It was lying about 70 cm below the surface, very close to a Dufour bladelet (Fig. S5), and it was covered by layer I, layer II and by the upper spits of layer III *(100, 101)*. As mentioned above, the level I is not diagnostic and the levels III and II include Protoaurignacian artefacts.

The deposit excavated in 1976 was thicker than in the neighbouring areas and partially cemented. The uppermost part of the deposit, corresponding to "layer I", formed a bulge in squares A1-B1. The 1976 field journal reports the following information on square B1: *"the central-front [NE] part of the square is occupied by a prominence, slightly to strongly cemented. [...] This thicker part was designated as layer I because its characteristics are very different from the top of square C1"* ("la parte centrale anteriore del quadrato è occupata da una serie in rialzo, mediamente o fort. (fortemente) concrezionata. […] Questo spessore maggiore è stato indicato come strato I in quanto presenta caratteristiche molto diverse dalla superficie di C1"). These statements are also confirmed by Vicino *(100)*, showing that later cementation by percolating $CaCO_3$ preserved the sediment from reworking.

Grotta di Fumane

Description of the site and history of the excavations

Grotta di Fumane (45.6° Lat, 10.9° Long) is situated in the Monti Lessini, a mountain group of the Veneto Alpine fringe; it lies at the base of a rock cliff at 350 m a.s.l., on the left of a small tributary stream flowing eastwards into the main Fumane Valley (Fig. S1). This important site was already known in the 19th century, and the first explorations were carried out by the Natural History Museum of Verona in 1964 and 1982, at the bottom of a sequence exposed by a road cut in 1950. New investigations started in 1988 *(16)*, under the patronage of the Superintendency for the Archeological Heritage of Veneto, and exposed a sequence of Palaeolithic occupation levels. Excavations are carried out yearly, since then, by the University of Ferrara.

The cave is part of a fossil karst complex excavated in the Ooliti di San Vigilio carbonatic sandstone (upper Lias), which is extensively dolomitized in the valley where the cave opens. The cave conjoins with other tunnels, and was completely obstructed by sediments and by the collapse of the external part of the roof. A sheltered area of almost 60 m^2 was unearthed after these rockfall deposits were removed, between 1990 and 1996, and extensive excavations were undertaken, with the aim of investigating evidence of the final Mousterian and Aurignacian occupations.

Stratigraphy

The whole cave complex preserves a sedimentary sequence 12 meters thick, divided from the bottom upwards into four macro-units labeled S, BR, A and D, which record the main climatic events that occurred between the Early and the Middle Würm *(106, 107)* (Fig. S6). Macro-unit A includes several horizontally layered beds from A13 to A1. Sediments from the Mousterian to the Aurignacian levels are mostly comprised of frost-shattered slabs with variable amounts of sand and aeolian dust, the former being prevalent in the western zone, the latter increasing progressively from the entrance to outside of the cave. Lithics, faunal remains, hearths and other structures embedding fine levels are densely scattered on the ground, particularly in units A11, A10, A9, A6-A5 (Mousterian) and A2, A1 (Protoaurignacian); conversely, less dense groups of these features, or isolated combustion structures and lithic workshops are preserved in units A5 (final Mousterian), A4, A3 (Uluzzian), D3, D1 (Aurignacian). The Late Mousterian and Uluzzian sequence and their cultural remains are described in several articles *(108-115)*. Layer A2 was excavated at different times since 1988 and over variable extensions in the area of the cave entrance. The most extensive investigations were carried out from 1988 to 2005. The archaeological material was either directly excavated using a 33 x 33 cm grid, or recovered from wet sieving. Macro-unit D tops the sequence and occludes the cavities, outlining the present-day slope morphology. Its origin is mainly due to several rockfall events, followed by stabilization and affected by cryoturbation. Human presence, was intense in the lower Aurignacian units (D3d, D3b and D3a), and became sporadic in the middle level D1d, in which some Gravettian artefacts were found *(116)*.

The discovery context of the human tooth

The tooth was found in square 91b (Fig. S7), well embedded in the sediment of unit A2. Layer A2 is a clearly discernible layer (preserved with variable thickness all over the cave entrance, from a few centimetres to 10 cm in thickness), due to its dark colour and its high charcoal, bone and stone implement density, and occurrence of dwelling structures (i.e. hearths, post-holes, waste dump areas). The stone implements are blades, retouched bladelets and Dufour bladelets. Other finds include bone and antler tools, painted stones (possibly parietal art), accumulations of ochre and over 800 mollusc shells *(117-121)*. A revised chronology of the Mid-Upper Palaeolithic sequence at the Grotta di Fumane *(10)* has shown that the start and the end of level A2 date respectively to 41,900-40,200 cal BP and 40,300-39,400 cal BP at the largest confidence interval.

Morphological description of the teeth

Bombrini

Lower left lateral deciduous incisor (Ldi_2) with partially-preserved crown and cervical quarter of the root (Fig. 1). The enamel is chipped off mesially, and there is a deep crack on the lingual side of the crown, which emanates from a second crack that runs mesio-distally. The incisal surface is worn, exposing a large area of dentine equivalent to wear stage 4 *(19)*. The crown appears asymmetrical in occlusal view, owing to a pronounced mesio-distal convexity that includes about two thirds of the labial and lingual surfaces, and to a slight concavity of the distal third. On the lingual side, there is a moderate lingual cervical eminence, but no tubercle-like structure; above this, the surface is concave, and shows faint mesial and distal marginal ridges, which reach the cervical eminence. An interproximal wear facet can be observed on the distal side, but not on the mesial one, and was probably removed by the mesial damage.

The preserved root stump is more elongated labially (4.1 mm) than lingually (1.6 mm), and appears to be resorptive, confirming an age of approximately 6 years on the basis of recent human standards *(122, 123)*. There is no evidence of either caries or enamel hypoplasia.

The tooth crown has a MD diameter of 4.3 mm (minimum estimation due to wear and mesial damage) and a BL diameter of 4.6 mm. At the cervix, the MD diameter is 3.2 mm and BL diameter is 4.4 mm. The computed Z-score for BL crown diameters shows that Bombrini is closer to the Upper Paleolithic modern humans mean (Table S1).

Fumane 2

Fumane 2 is an upper right lateral deciduous incisor (Rdi^2) with well-preserved crown and less than half of the root preserved (Fig. 1). A large fissure crosses the tooth mesio-distally, with a second one emanating from it towards the labial side. The incisal surface shows strong oblique wear (wear stage 6 according to ref. *(19)* from mesio-labial to disto-lingual. This wear removed nearly all the lingual enamel, except where it covers a lingual cervical prominence (not a tubercle-like structure). The labial border of the incisal edge is chipped, probably because of para-masticatory activities. The crown appears symmetrical

in occlusal view, and the preserved part of the labial surface is evenly and weakly convex mesio-distally. An interproximal wear facet can be observed on the distal side, but not on the mesial one, probably removed by wear.
The short segment of the root, longer labially (6.1 mm) than lingually (0.8 mm), looks resorptive, indicating an age of ~6/7 years on the basis of recent human standards *(122, 123)*.

The tooth crown has a MD diameter of 5.9 mm (minimum estimation due to wear) and a BL diameter of 5.5 mm (Table S1). At the cervix, MD is 4.2 mm and BL is 4.9 mm. The computed Z-score for BL crown diameters shows that Fumane 2 is closer to the Neandertal mean (Table S1).

As observed for other tooth classes *(2)*, the range of overlap in the crown dimensions of deciduous incisors makes them inappropriate for distinguishing modern humans from Neandertals. This explains why dental fossil remains retrieved decades ago and studied using crown diameters were often non-diagnostic or misclassified, as well as the reason to use state-of-the-art methods (such as enamel thickness and aDNA) for a reassessment of their taxonomic status.

3D enamel thickness of Bombrini

The values of the components of 3D enamel thickness computed for Bombrini and the comparative sample (Neandertals and recent modern humans) are summarized in Table 1 and reported in detail in Table S2. For each tooth, the wear stage was evaluated following ref. *(19)*.

When two recent modern human specimens are digitally worn down to the level of the Bombrini specimen, the AET index decreases of 0.04 mm and the RET index decreases of about 1 point, because tooth wear affects more the enamel volume than the dentine volume (Table S3). In addition, our results indicate that both AET and RET values remain quite stable when the artificially worn teeth are digitally damaged on the mesial side to simulate the condition observed in the Bombrini incisor, confirming both the reliability of the indices computed for Bombrini and that the original RET index (the index of the hypothetical unworn Bombrini incisor) should have been at least 1 point larger.

Ancient DNA

General characteristics of the libraries

The number of DNA molecules in each library, as quantified by digital droplet PCR, ranged between 3.8×10^9 and 1.7×10^{10} (Table S4), and were higher than extraction and library preparation negative controls in the experiments (not shown), consistent with a successful library preparation *(42)*. Following sequencing on a MiSeq (Illumina), the libraries yielded between 1.2 and 4.8 million reads (Table S4). For the libraries made from the first DNA extract (E1119), after discarding all sequences shorter than 35bp, 1.9%, 4.4% and 6.0% of sequences (from libraries L9358, A4678 and A4679, respectively) could be aligned with a mapping quality score >30 to the revised Cambridge Reference Sequence (Table S4). Each unique sequence was seen on average 6.2, 19.7 and 27.6 times for L9358, A4679 and A4678, respectively (Table S4), indicating that deeper sequencing would not substantially increase the yield of unique mitochondrial sequences. Libraries prepared from the second extract (E2748) yielded a substantially higher number (191,737 and 143,891 for L5184 and L5185, respectively) of unique mitochondrial sequences longer than 35bp, aligned with a mapping quality score higher than 30 (Table S4).

Nucleotide substitutions

The single-stranded ends of ancient DNA molecules tend to carry uracils (U) *(21, 22)*, which are the deamination product of cytosine (C) and are read as thymine (T) by DNA polymerases. The presence of C to T substitutions at the ends of DNA fragments, compared to the reference genome, can thus be used to determine whether they are of ancient origin (e.g., *(21-23, 55, 57, 58)*). All five libraries exhibit elevated frequencies of C to T substitutions near the start and end positions of the fragments, compared to the middle of the sequences and compared to any other type of nucleotide substitution (Fig. S9). In the two libraries (L5184 and L5185) prepared from the second DNA extract (E2748), 36-37% of Cs at the 5' end and 34-35% of Cs at the 3' end of the fragments appeared as Ts. These frequencies are comparable with sequences recovered from other ancient specimens of similar age *(23-26)*. The lower frequencies of C to T substitutions (14-17%) in the libraries produced from the first DNA extract (E1119) suggest that they contain a mixture of ancient and modern contaminating human DNA. Present-day DNA has been shown to be less affected by cytosine deamination than ancient DNA, when in untreated samples younger than 100 years old, only up to 10% of terminal Cs appeared as Ts *(22)*. The lowest C to T substitution frequency occurred at the 5' ends of sequences in library L9358. This is due to the pre-treatment of L9358 with *E. coli* UDG, which not only removes uracil bases from the interior of DNA molecules *(43, 44)*, but also from the ends of molecules, more efficiently so at the 5' than at the 3' end of molecules *(44)*.

Phylogenetic inferences based on 'diagnostic' positions

For the three libraries which yielded few mitochondrial DNA sequences (A4678, A4679 and L9358), in order to test whether they contain modern human or Neandertal mtDNA, we studied the state of sequences overlapping 63 'diagnostic' positions at which ten Neandertal mitochondrial genomes differ from 311 present-day humans. Out of 2,067 sequences overlapping these diagnostic positions, 2,063 matched the modern human state, and only four carried the Neandertal base (Table S5). After isolating sequences indicative of ancient DNA by retaining only sequences with terminal C to T substitutions, all fragments matched the modern human state (Table S5). The four sequences matching the Neandertal state may thus originate from sequencing errors.

In addition, in order to exclude the possibility that the sample originates from another hominin group, we analyzed 17 positions where modern humans are derived while Neandertals, Denisovans and a chimpanzee are ancestral. All but four fragments matched the modern human state (Table S5), and all fragments matched the modern human base after filtering for endogenous DNA fragments based on terminal C to T substitutions (Table S5).

Reconstructing the Fumane 2 mitochondrial genome

After merging the two libraries richest in unique mitochondrial sequences (L5184 and L5185), a mitochondrial genome of 1,013-fold coverage was reconstructed. Six mitochondrial positions were not called, as less than 80% of sequences overlapping them carried an identical base (Fig. S10). Two of these positions (302 and 310) are in the C-stretch of the mitochondrial D-loop, an area prone to misalignments due to multiple repetitions of the same base. The remaining four positions (5585, 7028, 16129 and 16304), however, were not due to misalignment, but rather to the presence of more than one type of mitochondrial sequences in the merged library. In order to discard likely contaminating sequences, we restricted further analyses to sequences carrying a terminal C to T substitution.

Using these sequences and with the above-mentioned parameters, we reconstructed a mitochondrial genome of 157-fold coverage (Fig. S10). Nine bases were not called. Two are positions 302 and 310 in the C-stretch, where a low consensus support is due to misalignment. These positions were fixed manually, by discarding sequences which showed misalignments to the reference genome. The remaining positions (1-4, 11, 16,566 and 16,569) are at or adjacent to the start and end of the reference genome. Since the mitochondrial genome is a circular molecule, while BWA can only use linear references, drops in coverage are expected at the junction point, i.e., near the first and last positions of the mitochondrial genome. These seven positions were fixed manually, as they are conserved in all mitochondrial genomes in our dataset. The full mitochondrial genome sequence of the Fumane 2 individual was deposited in GenBank (accession number KP718913).

Contamination estimate

The percentage of contaminating modern human DNA in our libraries was estimated by studying the state of sequences overlapping positions at which the Fumane 2 genome differs from the mitochondrial genomes of 311 present-day humans *(20)*. This analysis was restricted to sequences carrying a C to T substitution at their 5' and/or 3' position. Although there are no positions at which the Fumane 2 mitochondrial genome differs from all 311 present-day humans, it differs at two positions (5585 and 16304) from 90% of present-day human mtDNAs in our database. In the merged library used to determine the consensus genome (L5184 and L5185), 3 out of 79 sequences overlapping these two positions carry the present-day human base, resulting in a contamination estimate of 3.8%. We had little power to determine contamination in the remaining libraries, as few sequences overlap the two relevant positions. All sequences from libraries A4678 and A4679 (1 and 4 sequences, respectively) match the base in the Fumane 2 genome, while in L9358, only one out of two sequences carries the Fumane 2 base.

Haplogroup determination

We identified 14 polymorphic positions in the Fumane 2 mtDNA sequence. The Fumane 2 mitochondrial genome was assigned to haplogroup R with a quality of 94.4%. All expected mutations for this haplogroup (73G, 263G, 750G, 1438G, 2706G, 4769G, 7028T, 8860G, 11719A, 14766T and 15326G) were found in the Fumane 2 genome. The three remaining mutations (5585A, 16129A and 16304C) are known polymorphisms which are not associated with haplogroup R. The R haplogroup is one of three major non-African macro-haplogroups. Many haplogroups common today in Europe, the Near East, South Asia and East Asia are descendent lineages of haplogroup R *(27)*.

We investigated whether sequences in the three libraries which were not used to reconstruct the Fumane 2 genome concur with the assigned haplogroup. When analyzing all sequences in these libraries, between 0% and 54% of sequences overlapping a polymorphic site did not carry the mutation indicative of the R haplogroup (Table S6). After isolating sequences carrying a terminal C to T substitution, all sequences but one presented the base indicative of the R haplogroup (Table S6). It should be noted that this analysis has limited power, due to the low number of sequences overlapping one of the 11 polymorphic sites used to define the haplogroup.

Molecular dating

18 differences were found between the mtDNA sequence of Fumane 2 and that of a present-day Chinese individual, which falls in close proximity to Fumane 2 in the phylogenetic analysis (Fig. 2). By aligning the genomes to a present-day San individual to determine the likely ancestral base, 15 of these mutations were inferred to have occurred on the branch leading to the present-day Chinese individual, whereas only three were inferred to have occurred on the Fumane 2 branch. The Fumane 2 mtDNA has thus accumulated fewer nucleotide substitutions than a related present-day mtDNA since the split from their most recent common ancestor, as expected for an ancient individual (*23, 25).* In the phylogenetic analysis, the accumulation of fewer substitutions is reflected by the shortening of the Fumane 2 branch, compared to the branches of related present-day humans (Fig. 2). Based on a mitochondrial mutation rate of $2.53*10^{-8}$ substitutions per site per year (95% HPD: $1.76\text{-}3.23*10^{-8}$) *(27)*, the shortening of the Fumane 2 branch was translated to a difference in time of 22,422-41,150 years, compared to a present-day human carrying related mtDNA.

The same analysis was performed to estimate the difference in time between the Fumane 2 individual and the Ust-Ishim individual, an ancient modern human directly dated to 46,880-43,210 cal BP *(26)*, whose branch is shortened compared to Fumane 2 (Fig. 2). Based on a single difference between the two mitochondrial genomes, which is inferred to have occurred on the branch leading to Fumane 2, we estimate that the Fumane 2 individual is younger than the Ust-Ishim individual by 1,869-3,429 years.

The tip date for the Fumane 2 branch was estimated in a Bayesian framework, using 10 directly dated ancient modern humans *(25, 26)* as multiple calibration points. Following a MCMC run with 24,000,000 iterations using a constant population size and a relaxed clock model, the date of the Fumane 2 terminal node was estimated to be 44,599 (95% HPD: 19,755-72,070) years BP. It should be noted that three parameters in the model (the shape of the gamma distribution, the mean of branch rates and the total number of substitutions per site over time) had an effective sampling size (ESS) lower than 200, contributing to the uncertainty of this result.

When taking into account the large confidence intervals, the age of the Fumane 2 individual as estimated based on its mtDNA coincides with the chronometric data for the layer in which the Fumane 2 specimen was found, of 41,110-38,500 cal BP *(10)*.

Radiocarbon dating

Vicino 1976 excavation: Results and Discussion

Five samples from the G. Vicino excavation, from layer III to layer I, were dated. The radiocarbon results of the Protoaurignacian level (III and II) range from 33,980±160 to 29,950±260 ^{14}C BP. The bone sampled for level I, which is associated with Upper Palaeolithic material culture (albeit not diagnostic of the Protoaurignacian), dates to 29,660±250 ^{14}C BP. In this case, to better constrain the chronology of this excavation, the recently published dates on shells from the Mousterian deposit (level IV Table S8) *(4)* were included in the Bayesian model. Moreover, previous radiocarbon dates for Grotta di Fumane (Table S9) *(10)* were included in the OxCal 4.2 model, recalibrated with IntCal13, as a separate plot.

The overall Agreement index is 70.5% well above the minimal acceptable level of 60%. No outliers were detected when the t-type outlier analysis was performed, thus confirming the integrity of the sequence and the reliability of the chronology. The start calibrated boundary for the Mousterian level (level IV) ranges between 44,840 and 43,160 cal BP. The transition between the Mousterian level IV and the Protoaurignacian level II ranges between 40,710 and 34,190 cal BP. The age of the tooth from Bombrini, found in the level III, ranges between 40,710 and 35,640 cal BP in the model created by OxCal. However, given the two determinations for level III (MAMS-21663; ^{14}C Age 32,920±140 and MAMS-21662; ^{14}C Age 33,980±160), we believe that the tooth dates more likely to the unmodelled calibrated range from 38,670 to 36,560 cal BP. The Upper Palaeolithic part (level I) is calculated between 33,710 to 32,660 cal BP.

Excavation 2002-2005: Results and Discussion

The chronology of the deposits excavated in 2002-2005 is more complicated to establish (Fig. S11, Table S10). In this case, the outlier analysis detected three outliers (ca. 100%) in level A2: sample MAMS-21353 was identified as a 100% outlier, given its very young age. The Agreement index for the sequence is below the minimal acceptable level of 60% (A_overall 18.1%). These parameters already indicate disturbance in the more recently excavated area, as confirmed by the micromorphological evidence for mixing in the stratigraphy described above.

It is, therefore, difficult to state the true upper boundary of the Protoaurignacian for this part of the Riparo Bombrini deposits, due to the possible later disturbance produced by the Gravettian occupation. There is no clear evidence of diagnostic Gravettian assemblages in these layers, although some knapping by-products could be Gravettian. For this reason, we prefer to provide only the lower boundary for this excavation area, which is comprised between 40,820 and 38,380 cal BP at 68.2% of confidence and

42,280 and 37,630 at 95.4%. These results are in agreement with the dates produced on organic remains from the G. Vicino excavation of 1976.

Final remark

Another open question is whether the Protoaurignacian predates or is contemporaneous with a second dispersal of AMH north of the Alps bearing Early Aurignacian culture *(32)*. Some authors *(32)* have suggested that the Protoaurignacian culture spread first, disappeared during the extremely cold and dry conditions of Heinrich Stadial 4 *(35)*, and was eventually replaced by Early Aurignacian populations. On the basis of its chronological sequence, the fossil and archeological evidence from Riparo Bombrini challenge this hypothesis. At this site and at the adjacent Riparo Mochi *(8)*, Protoaurignacian populations lasted until ~34,000 cal BP (Table S8) and it can, therefore, not be argued that the Early Aurignacian culture represents an adaptive change in response to the climatic deterioration of Heinrich Stadial 4. Instead, it is conceivable that the Protoaurignacian and the Early Aurignacian represent contemporaneous widespread dispersals of AMH into Europe *(9)*.

Fig. S1. Geographical distribution of the Protoaurignacian. The human remains associated with the Protoaurignacian, and considered in this study, were unearthed from Riparo Bombrini (Ventimiglia, Italy) and Grotta di Fumane (Western Lessini Mountains, Italy).

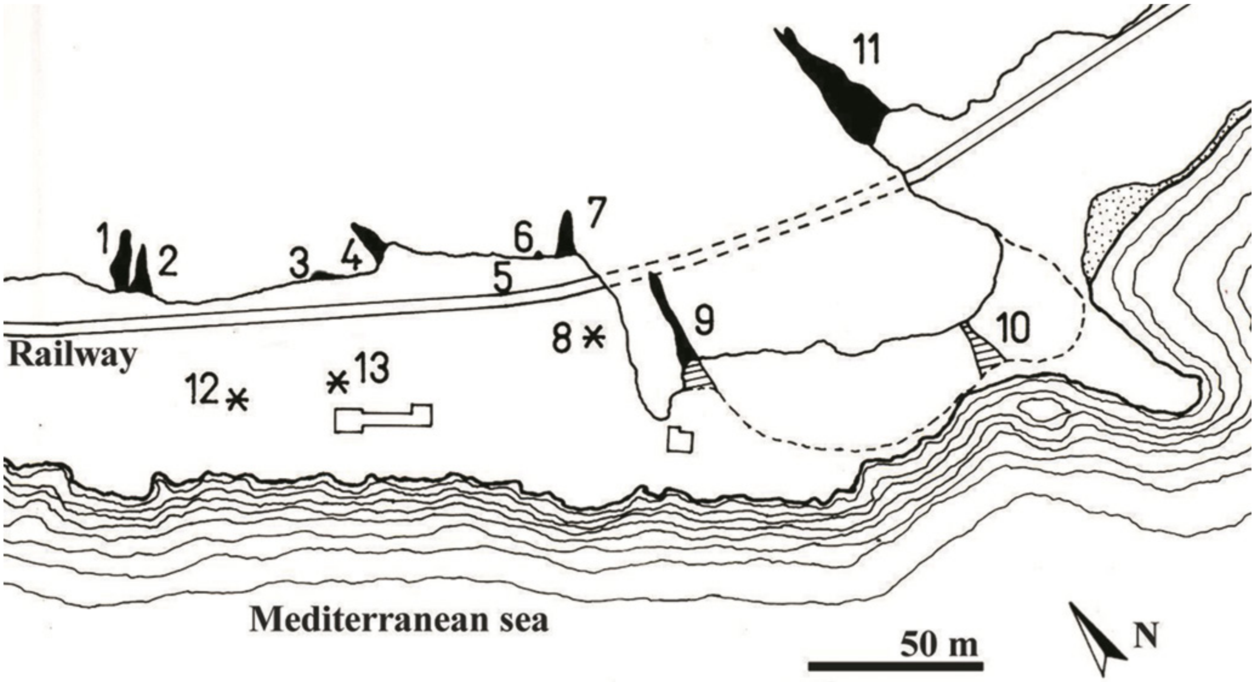

Fig. S2. The archaeological area of Balzi Rossi. Location of the sites: 1: Grotta Costantini; 2: Grotta dei Fanciulli; 3: Riparo Lorenzi; 4: Grotta di Florestano; 5: Riparo Mochi; 6: Riparo Blanc-Cardini; 7: Grotta del Caviglione; 8: Riparo Bombrini; 9: Barma Grande; 10: Grotta del Bausu da Ture; 11: Grotta del Principe; 12: site of the Ex-Casinò; 13: site of the Ex-Birreria (Drawing by Negrino, F.; modified from ref. *(124)*).

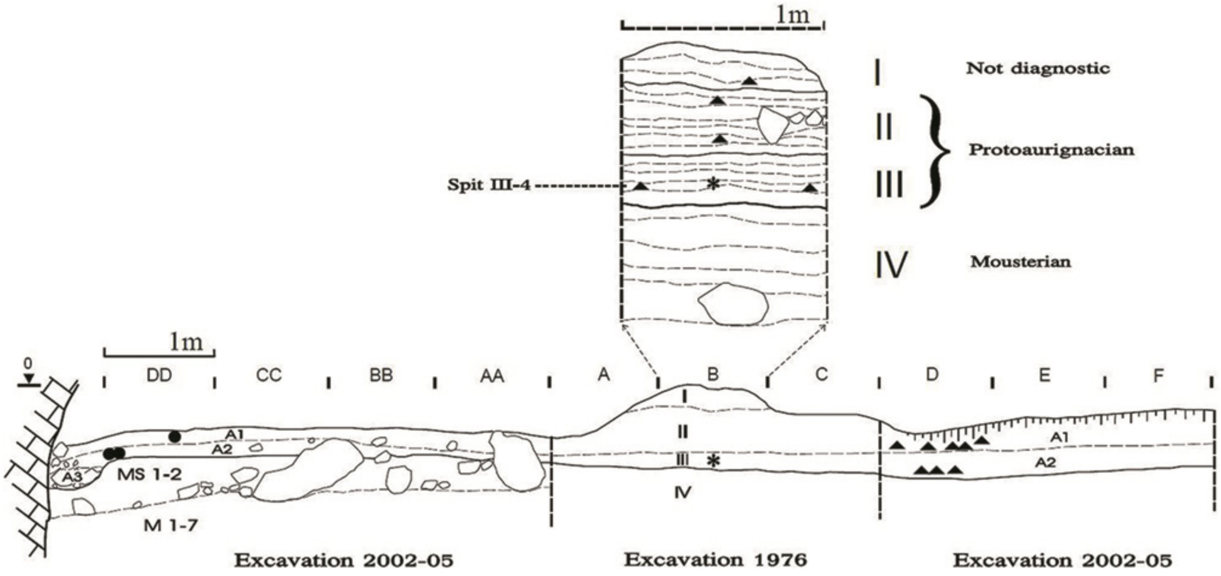

Fig. S3. Stratigraphic sequence of Riparo Bombrini. The asterisk indicates the position of the human tooth (level III - spit 4); triangles and circles indicate respectively the location of dated bone and charcoal samples (drawing by F. Negrino).

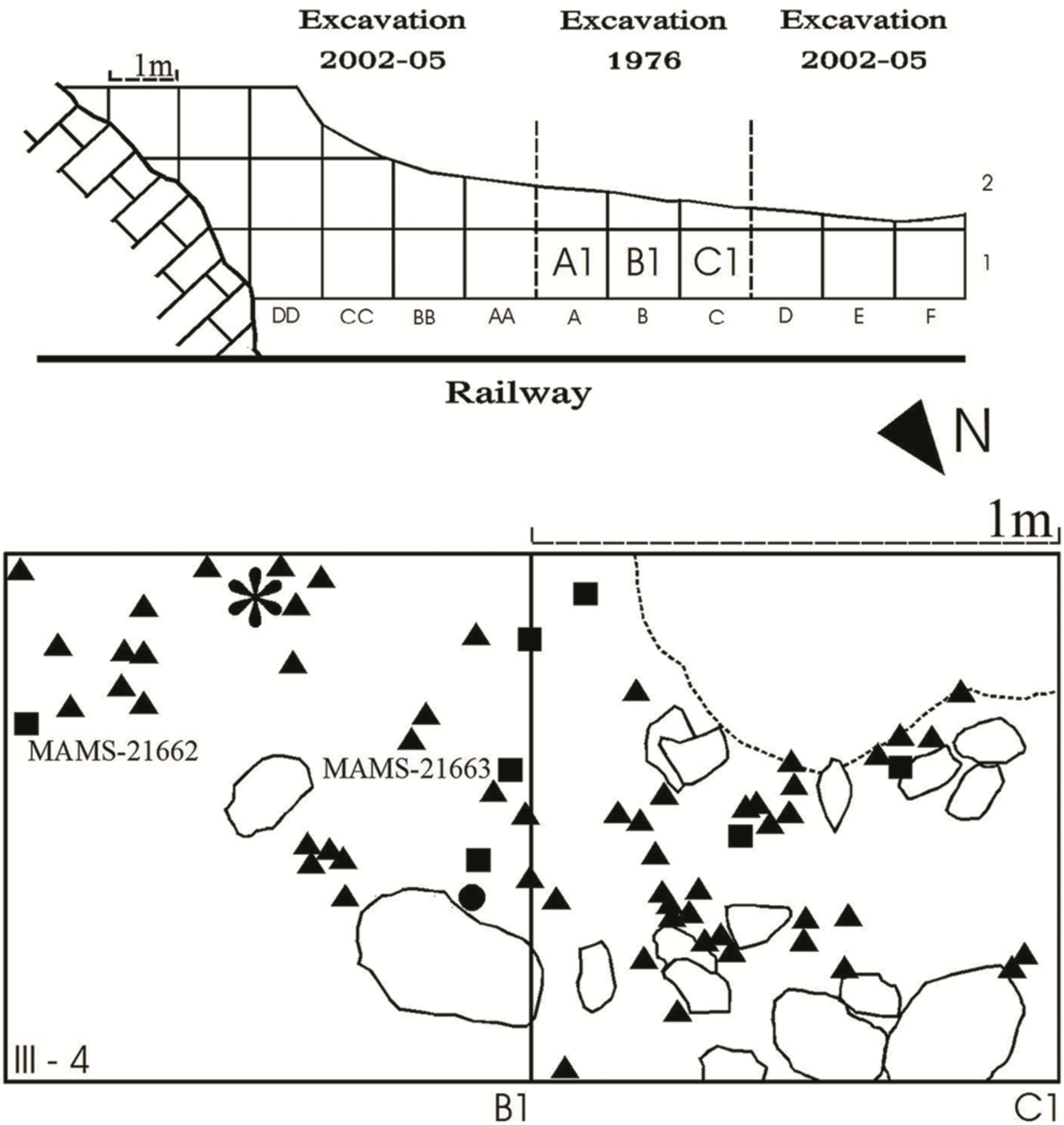

Fig. S4. Plan of the excavated area (above) and detail of squares B1-C1, Level III-spit 4, including mapped finds (below), Riparo Bombrini. Human tooth (asterisk), flint artefacts (triangles), red ochre (circle) and bones (squares), two of which dated (MAMS-21662 and MAMS-21663) (drawing by F. Negrino; modified from ref. *(97)*).

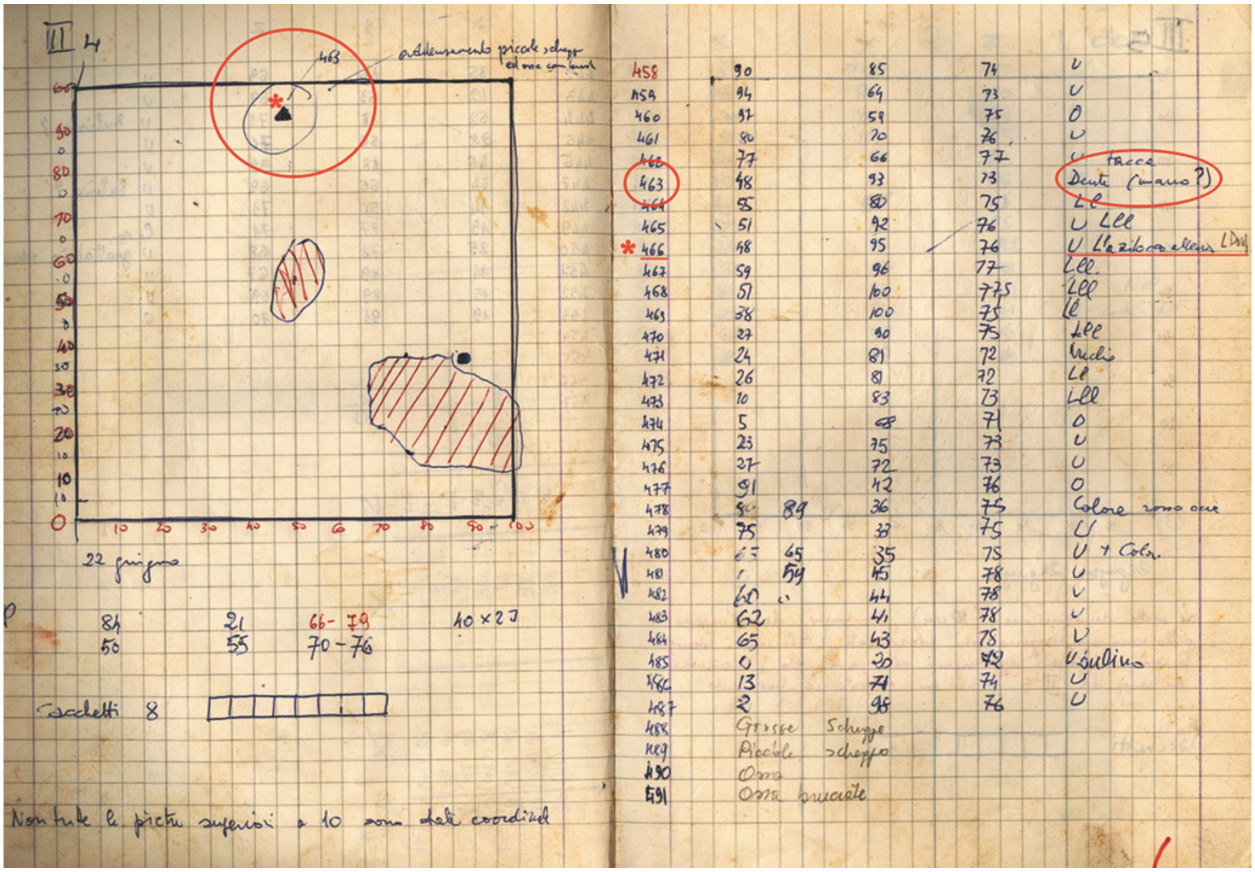

22 giugno

84 / 50 21 / 55 66 - 79 / 70 - 76 40 × 27

Sacchetti 8

Non tutte le pietre superiori a 10 sono state coordinate

458	90		85	74	U
459	94		64	73	U
460	97		59	75	O
461	80		70	76	U
462	77		66	77	U tracce
463	48		93	73	Dente (umano?)
464	55		80	75	Ll
465	51		92	76	U Lll
466	48		95	76	U [illegible] LDuf
467	59		96	77	Lll
468	51		100	77,5	Lll
469	38		100	75	Ll
470	27		90	75	Lll
471	24		81	72	Nucleo
472	26		81	72	Ll
473	10		83	73	Lll
474	5		68	71	O
475	23		75	73	U
476	27		72	73	U
477	91		42	76	O
478	90	89	36	75	Colore rosso ocra
479	75		33	75	U
480	65	65	35	75	U + Colo.
481	[illegible]	54	45	78	U
482	60		44	78	U
483	62		41	78	U
484	65		43	78	U
485	0		20	72	U bulino
486	13		71	74	U
487	2		98	76	U
488	Grosse schegge				
489	Piccole schegge				
490	Ossa				
491	Ossa bruciate				

Fig. S5. The 1976 field journal by Giuseppe Vicino, illustrating square B1, Level III-spit 4, Riparo Bombrini. The triangle (n.463) indicates the human tooth, while the asterisk marks a Dufour bladelet (n.466).

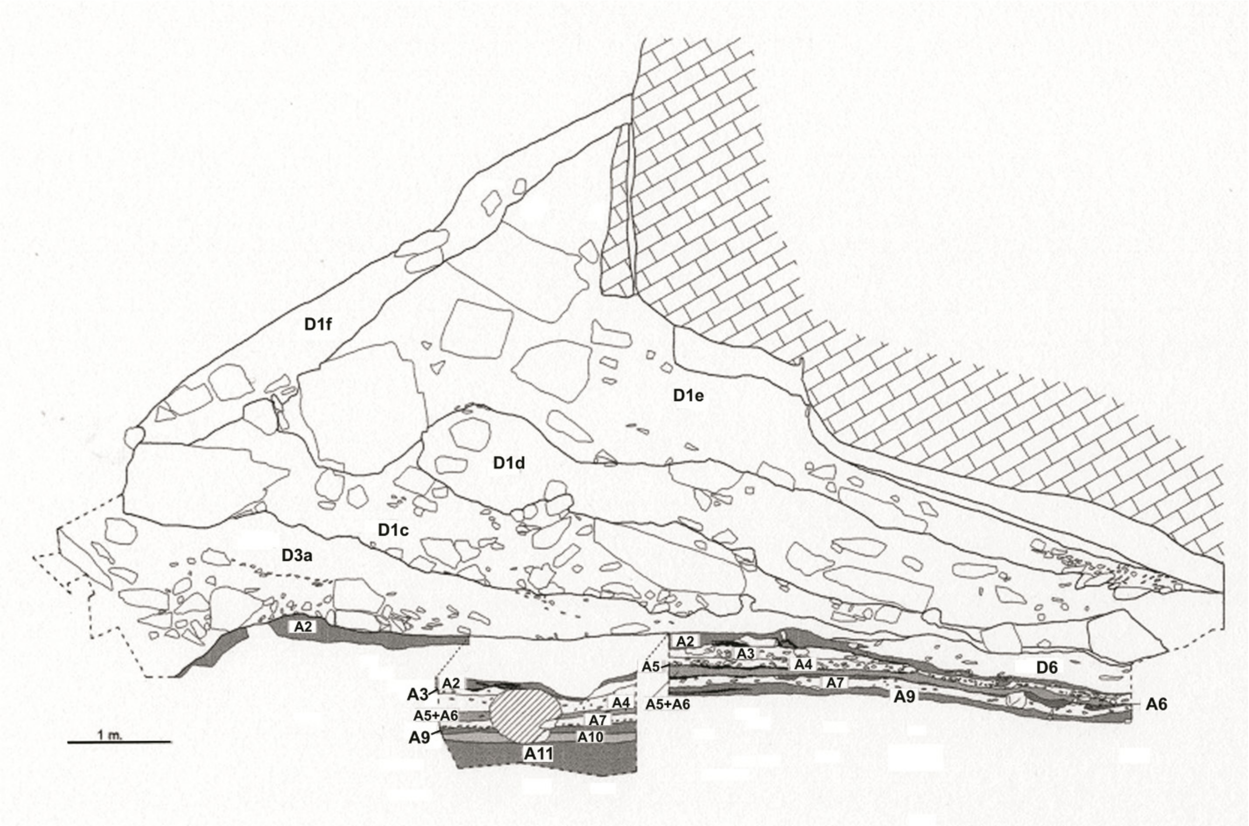

Fig. S6. Stratigraphic profile of Grotta di Fumane. Sketch section with evidence of late Mousterian (A11-A5), Uluzzian (A4-A3) and Protoaurignacian layers (A2), with variable content of archaeological remains (increasing from light gray to dark gray and black). (by M. Cremaschi, M. Peresani, redrawn by S. Muratori).

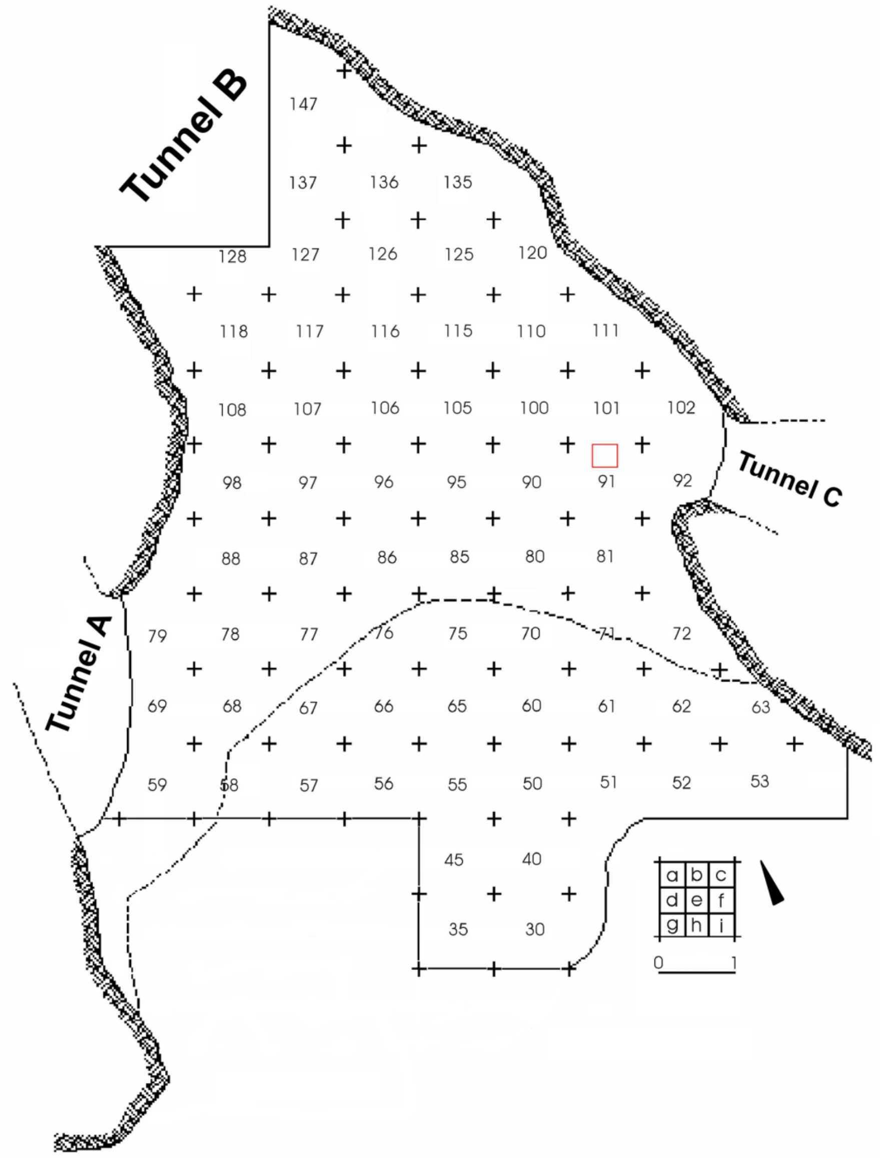

Fig. S7. Map of the excavated area of Grotta di Fumane. The red square marks the finding locus of the Fumane 2 specimen (square 91b). The dotted line shows the present-day entrance of the cave.

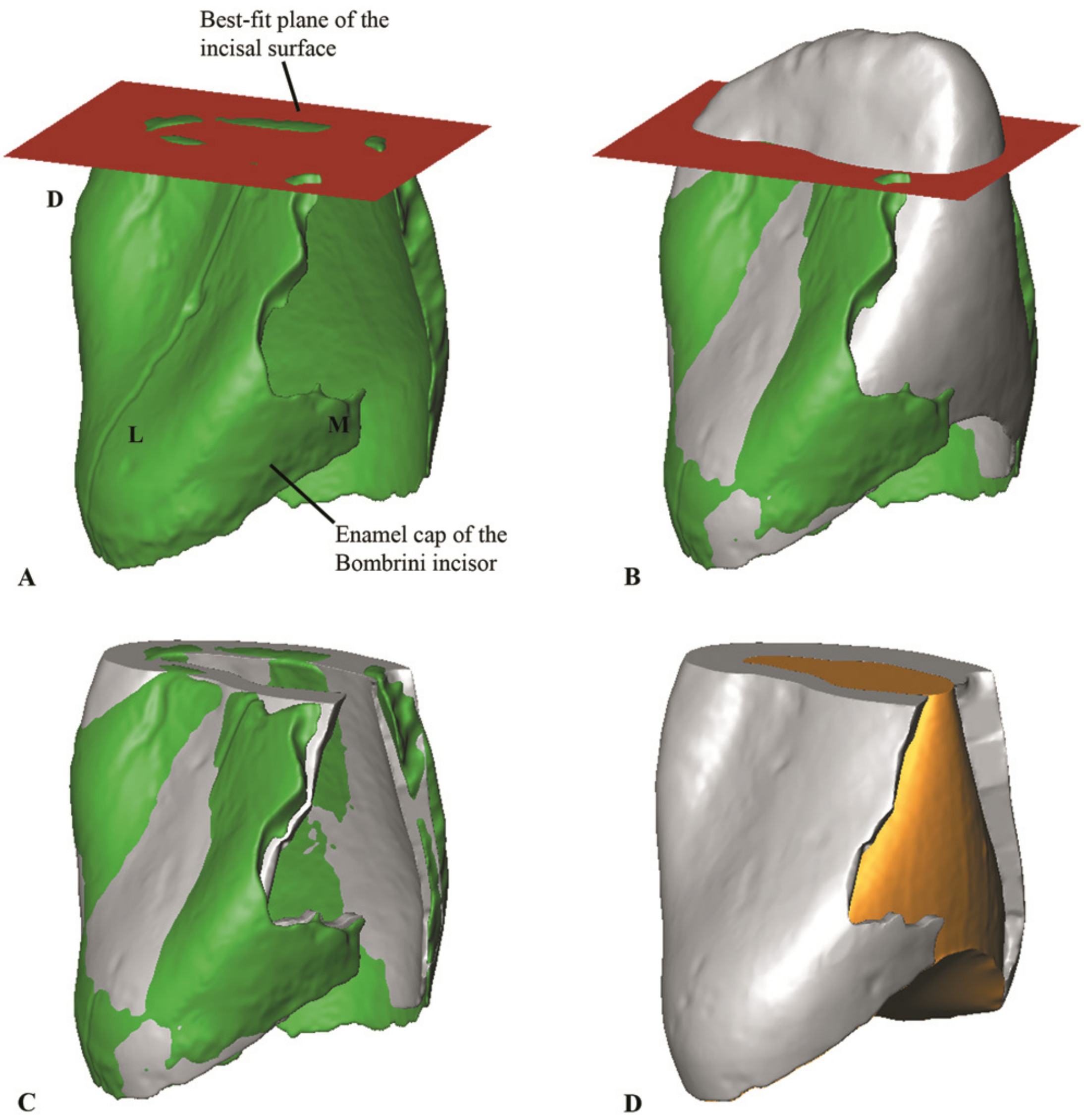

Fig. S8. Digital simulation of tooth wear and mesial damage in a modern human lower left lateral deciduous incisor (Ldi$_2$). A, A best-fit plane was interpolated on the incisal surface of the Bombrini Ldi$_2$**. B,** A modern human Ldi$_2$ (ID: SGVALD_T59) was superimposed to the Bombrini specimen using Iterative Closest Point algorithm. **C,** The portion of crown above the incisal plane and the portion of enamel in correspondence to the Bombrini's mesial damage were removed. **D,** The modern human specimen SGVALD_T59 virtually worn and damaged as the Bombrini Ldi$_2$. D, distal; L, lingual; M, mesial.

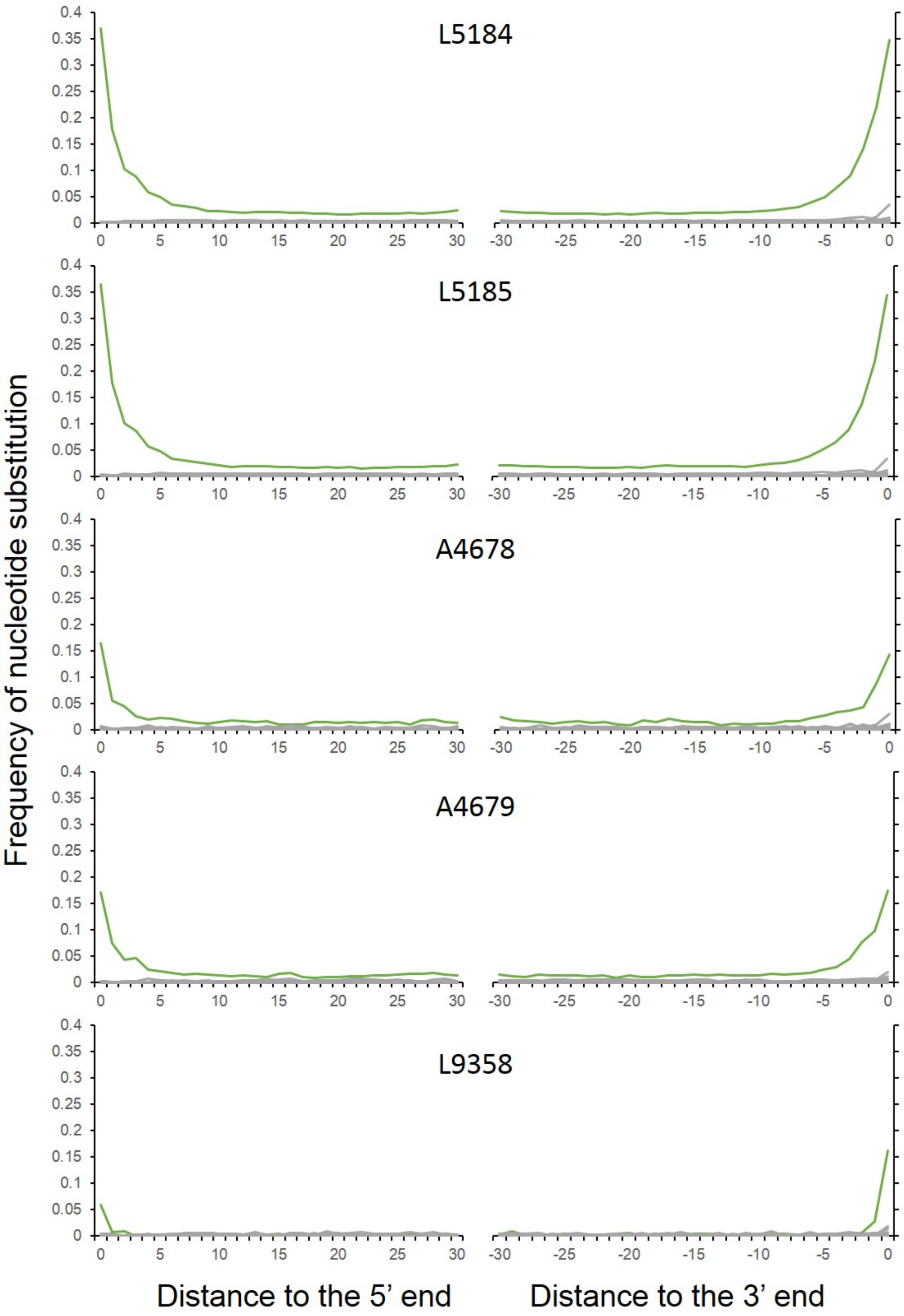

Fig. S9. Frequencies of nucleotide substitutions at the start and end positions of sequences from Fumane 2, per DNA library. C to T substitution frequencies are marked in green. Note that the C to T substitutions are only elevated at or adjacent to the start and end positions of the sequences. All other types of nucleotide changes are marked in gray.

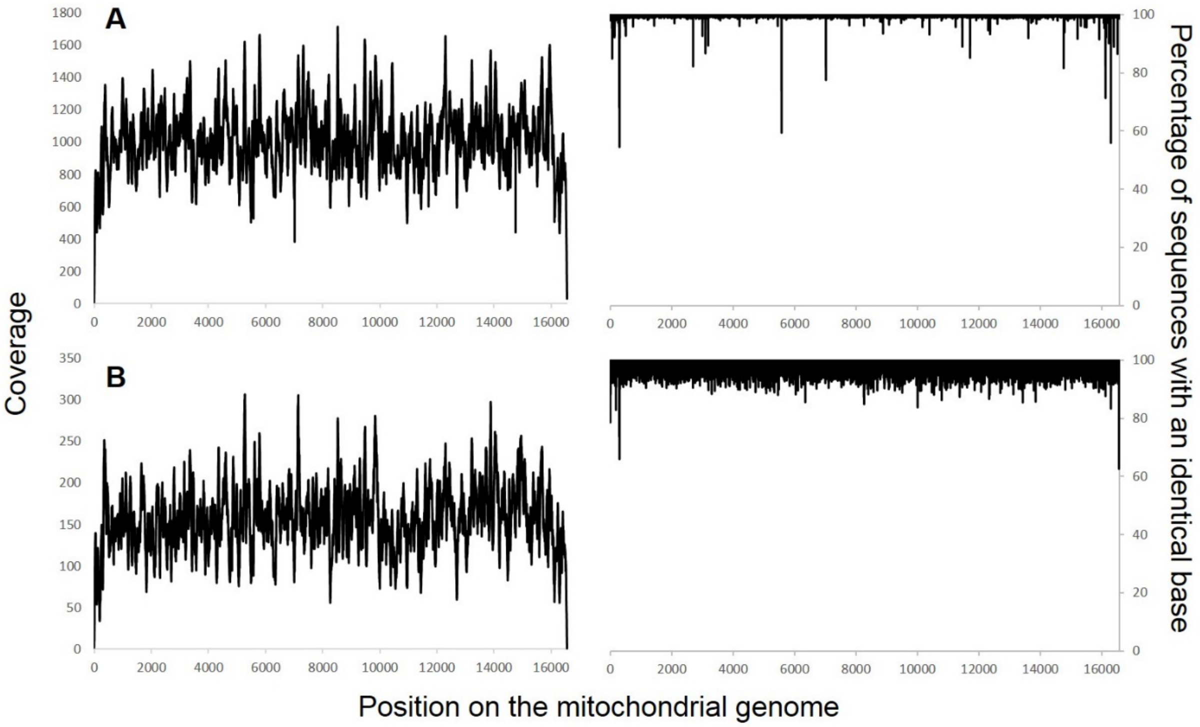

Fig. S10. Reconstructing the Fumane 2 mitochondrial genome. Plots show the number of sequences overlapping each position in the mitochondrial genome (coverage, left side) and the percentage of sequences carrying an identical base (right). Results are shown for all sequences (A), and after retaining only sequences with a terminal C to T substitution (B).

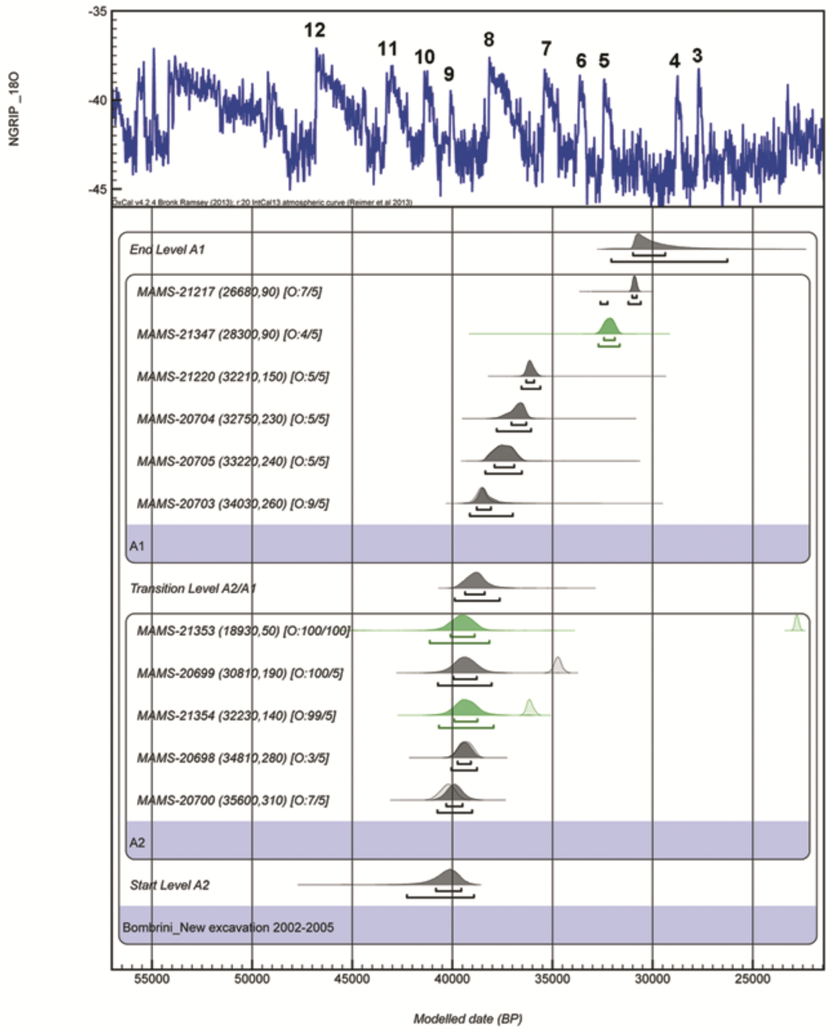

Fig. S11. Bayesian model of dates on organic remains from the 2002-2005 excavations at Riparo Bombrini. Radiocarbon dates are calibrated in IntCal13 *(29)*. Model and boundaries were computed by OxCal 4.2 *(34)*, including the performance of the General t-type Outlier Model *(34)*. Bone samples treated with ultrafiltration in grey; charcoal samples treated with ABOX in green. The results are linked with the (NGRIP) δ^{18}O climate record *(74, 75)*.

Table S1. Buccolingual (BL) diameters. Dental dimensions (in mm) of Bombrini and Fumane 2 standardized to Z-scores of the hominin samples[a-c] used in this study (m=mean; s=standard deviation; n=number of individuals).

	Bombrini (di_2)		Fumane 2 (di^2)	
	BL		BL	
	m ± s (n)	Z score	m ± s (n)	Z score
	4.6		5.5	
N	4.85±0.25 (15)[a]	-1.00	5.38±0.48 (9)[b]	0.25
UPMH	4.58±0.30 (18)[a]	0.07	5.12±0.29 (5)[b]	1.31
RMH	4.14±0.37 (62)[a]	1.24	4.7±0.4 (69)[c]	2.00

Based on [a]ref. *(125)*, [b]ref. *(126)* and [c]ref. *(127)*; N=Neandertals; UPMH=Upper Palaeolithic modern human; RMH=recent modern human

Table S2. Three-dimensional enamel thickness. Values of the components of 3D enamel thickness of Bombrini, Neandertals and recent modern human (RMH) lower lateral deciduous incisors (di_2).

Taxon	Specimen ID	Side	Wear stage[a]	Enamel volume (mm^3)	Coronal dentine + pulp volume (mm^3)	EDJ[b] surface (mm^2)	3D AET[c] (mm)	3D RET[d] (scale-free)
Bombrini		L	4	10.87	31.01	37.53	0.29	9.22
Neandertals	Abri Suard	R	3	18.64	58.89	73.03	0.26	6.56
	Amud 7	L	1	21.14	50.93	69.59	0.30	8.20
	Kebara 1	L	2	20.25	52.24	71.89	0.28	7.54
	La Ferrassie 8	L	1	19.47	46.95	68.24	0.29	7.91
	Roc de Marsal 1	R	3	16.85	47.22	63.53	0.27	7.34
RMH	Guid T8	L	4	11.58	27.11	44.03	0.26	8.75
	Guid T20	R	4	10.66	30.82	48.70	0.22	6.98
	Guid T22	R	4	14.80	28.57	46.54	0.32	10.40
	Guid T38	L	3	11.00	26.50	46.07	0.24	8.01
	Guid T39	R	2	18.11	31.61	52.21	0.35	10.97
	Guid T41	L	3	15.85	32.98	49.23	0.32	10.04
	Guid T49B	R	4	11.90	27.92	45.97	0.26	8.53
	Guid TB65	L	3	11.77	26.47	46.09	0.26	8.57
	Roccap US26	R	2	16.40	27.75	46.02	0.36	11.77
	Sgvald T37	R	3	13.74	27.85	47.10	0.29	9.62
	Sgvald T53	L	3	16.98	35.06	55.88	0.30	9.28
	Sgvald T54	L	3	15.53	26.69	46.40	0.33	11.20
	Sgvald T59	R	2	15.80	27.47	45.57	0.35	11.49
	Vald_BC TB75	L	3	17.21	33.23	51.33	0.34	10.43
	Vald T64	L	3	14.96	28.18	46.45	0.32	10.58
	Vald TB43	R	3	13.81	29.23	48.62	0.28	9.22
	Vald TB72	L	3	15.07	25.29	43.33	0.35	11.85
	Vald TB124	L	3	17.27	29.46	50.95	0.34	10.97

[a]Based on ref. *(19)*; [b]EDJ=enamel-dentine junction; [c]AET=average enamel thickness index; [d]RET=relative enamel thickness index

Table S3. Three-dimensional enamel thickness of two recent modern human specimens (Guid_T39 and Sgvald_T59). The specimens were digitally worn and damaged to simulate the condition of the Bombrini incisor.

Specimen ID	Simulation	Enamel volume (mm^3)	Coronal dentine + pulp volume (mm^3)	EDJ[a] surface (mm^2)	AET[b] (mm)	RET[c] (scale-free)
Guid_T39	Original	18.11	31.61	52.21	0.35	10.97
	Bombrini's wear stage	13.17	29.71	43.08	0.31	9.87
	Bombrini's wear stage and damage	10.86	29.71	36.11	0.30	9.71
Sgvald_T59	Original	15.80	27.47	45.57	0.35	11.49
	Bombrini's wear stage	12.87	26.73	40.92	0.31	10.52
	Bombrini's wear stage and damage	11.14	26.73	35.2	0.32	10.58

[a]EDJ=enamel-dentine junction; [b]AET=average enamel thickness index; [c]RET=relative enamel thickness index

Table S4. General characteristics of the five DNA libraries generated.

Library ID	Extract ID	Extract used (µl)	USER treated	Molecules in library (ddPCR estimate)	Number of raw sequences	Number of aligned sequences	Sequences mapped [%]	Number of unique sequences	Average number of duplicates	Number of sequences with C to T substitution
A4678	E1119	5	-	3.78E+09	2,902,307	129,057	4.4	4,590	27.6	280
A4679	E1119	15	-	9.40E+09	3,204,305	196,103	6.0	9,722	19.7	686
L9358	E1119	10	+	1.66E+10	1,176,132	21,953	1.9	3,531	6.2	141
L5184	E2748	10	-	6.08E+09	4,783,591	1,282,388	25.4	191,737	6.4	32,405
L5185	E2748	10	-	6.02E+09	4,720,141	342,251	6.9	143,891	2.3	23,515

C, cytosine; T, thymine

Table S5. Number of mtDNA sequences overlapping phylogenetically diagnostic positions. Number of sequences matching the modern human base in two sets of diagnostic positions, before and after filtering for sequences with terminal C to T substitutions. Set 1 includes 63 positions at which modern humans differ from Neandertals. Set 2 includes 17 positions at which modern humans differ from Neandertals, Denisovans and a chimpanzee

		Set 1		Set 2	
Library ID	Total number of mtDNA sequences	Number of human diagnostic sequences	Number of Neandertal diagnostic sequences	Number of human diagnostic sequences	Number of Nea/Den/Pan diagnostic sequences
All mtDNA sequences					
A4678	4,590	537	0	128	0
A4679	9,722	1,146	4	284	4
L9358	3,531	380	0	109	0
Sum	17,843	2,063	4	521	4
Sequences with a terminal C to T substitution					
A4678	280	16	0	4	0
A4679	686	53	0	10	0
L9358	141	13	0	2	0
Sum	1,107	82	0	16	0

mtDNA, mitochondrial DNA; Nea, Neandertal; Den, Denisova; Pan, chimpanzee (*Pan troglodytes*); C, cytosine; T, thymine

Table S6. Number of mtDNA sequences overlapping polymorphic positions indicative of haplogroup R. Results are shown for all sequences in a DNA library, and after retaining only sequences with terminal C to T substitutions

	Library A4678		Library A4679		Library L9358	
Polymorphism indicative of haplogroup R	Number of sequences with base indicative of R haplogroup	Number of sequences with other base	Number of sequences with base indicative of R haplogroup	Number of sequences with other base	Number of sequences with base indicative of R haplogroup	Number of sequences with other base
All mtDNA sequences						
73G	22	6	35	22	6	7
263G	18	0	31	0	13	0
750G	20	1	30	0	11	0
1438G	24	1	44	1	7	0
2706G	13	2	23	9	5	3
4769G	20	0	28	0	15	0
7028T	10	4	16	12	5	0
8860G	14	2	33	0	7	0
11719A	14	2	34	5	10	3
14766T	17	6	27	6	16	6
15326G	13	0	41	1	10	0
Sum	185	24	342	56	105	19
Sequences with a terminal C to T substitution						
73G	NA	NA	2	0	NA	NA
263G	NA	NA	1	0	NA	NA
750G	0	1	4	0	1	0
1438G	NA	NA	1	0	1	0
2706G	NA	NA	1	0	NA	NA
4769G	NA	NA	1	0	NA	NA
7028T	NA	NA	2	0	1	0
8860G	NA	NA	3	0	NA	NA
11719A	1	0	4	0	NA	NA
14766T	2	0	1	0	2	0
15326G	NA	NA	3	0	NA	NA
Sum	3	1	23	0	5	0

mtDNA, mitochondrial DNA; C, cytosine; T, thymine; G, guanine; A, adenine; NA, no sequences overlap the position.

Table S7. AMS radiocarbon results of 16 samples from Riparo Bombrini from the 2002-2005 and 1976 excavations. For the bone samples we included the isotopic values, C:N ratios and the amount of collagen extracted (%Coll), which refer to the >30 kDa fraction. $\delta^{13}C$ values are reported relative to the vPDB standard and $\delta^{15}N$ values are reported relative to the AIR standard. The humanly modified bones are indicates by an * next to the MPI Lab Code.

New Excavations (2002-2005)													Cal BP from	Cal BP to	Cal BP from	Cal BP to
MPI Lab Nr.	**Square nr.**	**U.S.**	**Material**	**% Coll**	**$\delta^{13}C$**	**$\delta^{15}N$**	**%C**	**%N**	**C:N**	**AMS nr.**	**^{14}C Age**	**1σ Err**	**68.20%**		**95.40%**	
S-EVA 29022	D1-III/3	Level A1	Bone	1.2	-19.6	5.4	45.2	15.8	3.3	MAMS-20703	34,030	260	38,830	38,280	39,170	37,810
S-EVA 29026	D1-III/3 16 nº62	Level A1	Bone	0.7	-19.3	6.3	41.9	14.6	3.4	MAMS-20705	33,220	240	37,910	36,940	38,300	36,640
S-EVA 29023	D1-III/3 13 nº14	Level A1	Bone	1.3	-19.0	5.9	39.8	14.0	3.3	MAMS-20704	32,750	230	37,020	36,320	37,630	36,150
S-EVA 29021	D1-III/2 22 nº31	Level A1	Bone	1.1	-19.4	4.9	44.3	15.4	3.4	MAMS-21220	32,210	150	36,300	35,940	36,440	35,720
S-EVA 29194*	D1 III/3 76 20	Level A1	Bone	1.0	-19.3	4.2	36.7	12.3	3.5	MAMS-21217	26,680	90	31,000	30,800	31,080	30,700
S-EVA-29889	DD1 III 1 n.24	Level A1	Charcoal							MAMS-21347	28,300	90	32,430	31,890	32,650	31,690
S-EVA 29017*	D1-III/5 nº133	Level A2	Bone	1.4	-19.0	5.6	43.1	15.7	3.2	MAMS-20700	35,600	310	40,590	39,830	41,010	39,490
S-EVA 29015	D1-III/5 16	Level A2	Bone	1.7	-19.4	5.1	43.0	15.7	3.2	MAMS-20698	34,810	280	39,670	38,960	40,010	38,680
S-EVA 29016	D1-III/5 17	Level A2	Bone	0.8	-19.2	6.8	43.1	15.5	3.2	MAMS-20699	30,810	190	34,930	34,540	35,130	34,310
S-EVA-29895	DD1 III 3a n.99	Level A2	Charcoal							MAMS-21354	32,230	140	36,310	35,960	36,450	35,750
S-EVA-29894	DD1 III 3a n.97	Level A2	Charcoal							MAMS-21353	18,930	50	22,900	22,700	22,970	22,600

Vicino Excavation (1976)													Cal BP from	Cal BP to	Cal BP from	Cal BP to
MPI Lab Nr.	**Square nr.**	**U.S.**	**Material**	**% Coll**	**$\delta^{13}C$**	**$\delta^{15}N$**	**%C**	**%N**	**C:N**	**AMS nr.**	**^{14}C Age**	**1σ Err**	**68.20%**		**95.40%**	
S-EVA-30845	B1 I/3 N33	Level I	Bone	0.9	-19.6	7.8	34.7	12.8	3.2	MAMS-22272	29,660	250	34,030	33,610	34,290	33,360
S-EVA-30847	B1 II/3	Level II	Bone	0.7	-19.8	5.4	40.3	14.4	3.3	MAMS-22273	31,780	320	36,050	35,330	36,330	34,980
S-EVA-30849	B1 II/7	Level II	Bone	0.7	-19.3	4.6	26.7	9.7	3.2	MAMS-22274	29,950	260	34,250	33,800	34,550	33,630
S-EVA-29896	B1 474 III 4	Level III	Bone	1.4	-19.2	6.5	44.1	14.9	3.5	MAMS-21662	33,980	160	38,670	38,340	38,870	38,110
S-EVA-29897	B1 460 III 4	Level III	Bone	0.9	-19.4	5.9	29.4	10.0	3.4	MAMS-21663	32,920	140	37,190	36,560	37,600	36,410

Table S8. AMS radiocarbon dating of Riparo Bombrini Mousterian level IV, published in ref. ***(4)*****.**

Square identification	Material	AMS nr.	^{14}C Age	1σ Err
Bomb 6-M3 IV,AA1 8 122	Shell	OxA-19862	40,340	390
Bomb 3-M5 IV,BB1 11	Shell	OxA-19291	38,140	260
Bomb 7-M3 IV,AA1 8	Shell	OxA-20361	36,770	210
Bomb 8-M2 IV, AA1 7	Shell	OxA-19292	36,540	240

Table S9. AMS radiocarbon dating of Grotta di Fumane Protoaurignacian level A2, published in ref. *(10)*.

Square identification	**Material**	**AMS nr.**	**^{14}C Age**	**1σ Err**
A2,struc.18	Charcoal	OxA-19584	35,850	310
A2,sq.97b	Charcoal	OxA-17569	35,640	220
A2,sq.107i	Charcoal	OxA-19570	35,180	220
A2,struc.17	Charcoal	OxA-19412	34,940	280
A2,struc.16/lev B	Charcoal	OxA-19414	34,180	270

Table S10. Calibrated boundaries for Riparo Bombrini (2002-2005 and Vicino 1976 excavations) and for the Protoaurignacian layers at Grotta di Fumane. The calibration was computed by OxCal 4.2 *(34)* using the International Calibration Curve IntCal13 *(29)* for terrestrial samples. The Marine 13 *(29)* calibration curve was used for the shell samples from the Mousterian level IV at Riparo Bombrini.

2002-2005 excavations	**Modelled (BP)**			
Indices **Amodel 17.1** **Aoverall 18.1**	**from**	**to**	**from**	**to**
	68.20%		**95.40%**	
End level A1	30,980	29,360	32,060	26,260
Transition level A2/A1	39,370	38,380	39,890	37,630
Start level A2	40,820	39,550	42,280	38,920

Vicino excavation (1976)	**Modelled (BP)**			
Indices **Amodel 67.6** **Aoverall 70.5**	**from**	**to**	**from**	**to**
	68.20%		**95.40%**	
End level I (Upper Palaeolithic)	33,990	32,660	34,150	30,140
Transition level II (Protoaurignacian) / level I(Upper Palaeolithic)	34,190	33,710	34,510	33,470
Transition level III/II (Protoaurignacian)	36,790	35,640	37,310	35,140
Transition level IV(Mousterian) / level III (Protoaurignacian)	40,710	38,940	40,960	38,460
Start level IV (Mousterian)	44,840	43,160	47,690	42,180

Fumane	**from**	**to**	**from**	**to**
Indices **Amodel 67.6** **Aoverall 70.5**	**68.20%**		**95.40%**	
Layer A2-A1	39,640	38,500	40,050	37,910
Protoaurignacian	40,430	39,200	41,470	38,410
Layer A3-A2	41,110	39,920	42,590	39,610

REFERENCES AND NOTES

1. J. F. Hoffecker, The spread of modern humans in Europe. *Proc. Natl. Acad. Sci. U.S.A.* **106**, 16040–16045 (2009). Medline doi:10.1073/pnas.0903446106

2. S. Benazzi, K. Douka, C. Fornai, C. C. Bauer, O. Kullmer, J. Svoboda, I. Pap, F. Mallegni, P. Bayle, M. Coquerelle, S. Condemi, A. Ronchitelli, K. Harvati, G. W. Weber, Early dispersal of modern humans in Europe and implications for Neanderthal behaviour. *Nature* **479**, 525–528 (2011). Medline doi:10.1038/nature10617

3. J.-J. Hublin, S. Talamo, M. Julien, F. David, N. Connet, P. Bodu, B. Vandermeersch, M. P. Richards, Radiocarbon dates from the Grotte du Renne and Saint-Césaire support a Neandertal origin for the Châtelperronian. *Proc. Natl. Acad. Sci. U.S.A.* **109**, 18743–18748 (2012). Medline doi:10.1073/pnas.1212924109

4. T. Higham, K. Douka, R. Wood, C. B. Ramsey, F. Brock, L. Basell, M. Camps, A. Arrizabalaga, J. Baena, C. Barroso-Ruíz, C. Bergman, C. Boitard, P. Boscato, M. Caparrós, N. J. Conard, C. Draily, A. Froment, B. Galván, P. Gambassini, A. Garcia-Moreno, S. Grimaldi, P. Haesaerts, B. Holt, M. J. Iriarte-Chiapusso, A. Jelinek, J. F. Jordá Pardo, J. M. Maíllo-Fernández, A. Marom, J. Maroto, M. Menéndez, L. Metz, E. Morin, A. Moroni, F. Negrino, E. Panagopoulou, M. Peresani, S. Pirson, M. de la Rasilla, J. Riel-Salvatore, A. Ronchitelli, D. Santamaria, P. Semal, L. Slimak, J. Soler, N. Soler, A. Villaluenga, R. Pinhasi, R. Jacobi, The timing and spatiotemporal patterning of Neanderthal disappearance. *Nature* **512**, 306–309 (2014). Medline doi:10.1038/nature13621

5. J.-G. Bordes, in *The Chronology of the Aurignacian and of the Transitional Technocomplexes: Dating, Stratigraphies, Cultural Implications*, J. Zilhão, F. D'Errico, Eds. (Instituto Português de Arqueologia, 2003), pp. 223–246.

6. O. Bar-Yosef, in *More than Meets the Eye: Studies on Upper Palaeolithic Diversity in the Near East*, A. N. Goring-Morris, A. Belfer-Cohen, Eds. (Oxbow Books, 2003), pp. 265–273.

7. P. Mellars, A new radiocarbon revolution and the dispersal of modern humans in Eurasia. *Nature* **439**, 931–935 (2006). Medline doi:10.1038/nature04521

8. K. Douka, S. Grimaldi, G. Boschian, A. del Lucchese, T. F. Higham, A new chronostratigraphic framework for the Upper Palaeolithic of Riparo Mochi (Italy). *J. Hum. Evol.* **62**, 286–299 (2012). Medline doi:10.1016/j.jhevol.2011.11.009

9. J-J. Hublin, The Modern Human Colonization of Western Eurasia: When and Where? *Quarter. Sci. Rev.* (2014); http://dx.doi.org/10.1016/j.quascirev.2014.08.011.

10. T. Higham, F. Brock, M. Peresani, A. Broglio, R. Wood, K. Douka, Problems with radiocarbon dating the Middle and Upper Palaeolithic transition in Italy. *Quat. Sci. Rev.* **28**, 1257–1267 (2009). doi:10.1016/j.quascirev.2008.12.018

11. C. A. Bergman, C. B. Stringer, Fifty years after: Egbert, an early upper Palaeolithic juvenile from Ksar Akil, Lebanon. *Paéorient* **15**, 99–111 (1989). doi:10.3406/paleo.1989.4512

12. N. J. Conard, P. M. Grootes, F. H. Smith, Unexpectedly recent dates for human remains from Vogelherd. *Nature* **430**, 198–201 (2004). Medline doi:10.1038/nature02690

13. S. Beckouche, F. Poplin, in *Le Piage, Site Préhistorique du Lot*, F. Champagne, R. Espitalié, Eds. (Société Préhistorique Française, 1981), pp. 159–160.

14. V. Formicola, Early aurignacian deciduous incisor from Riparo Bombrini at Balzi Rossi (Grimaldi, Italy). *Rev. Antropol.* **67**, 287–292 (1989).

15. Information on materials and methods and localities is available on *Science* Online.

16. G. Bartolomei *et al*., La Grotte-Abri de Fumane. Un Site Aurignacien au Sud des Alps. *Preistoria Alpina* **28**, 131–179 (1992).

17. S. Benazzi, D. Panetta, C. Fornai, M. Toussaint, G. Gruppioni, J. J. Hublin, Guidelines for the digital computation of 2D and 3D enamel thickness in hominoid teeth. *Am. J. Phys. Anthropol.* **153**, 305–313 (2014). Medline doi:10.1002/ajpa.22421

18. R. Macchiarelli, L. Bondioli, A. Debénath, A. Mazurier, J. F. Tournepiche, W. Birch, M. C. Dean, How Neanderthal molar teeth grew. *Nature* **444**, 748–751 (2006). Medline doi:10.1038/nature05314

19. S. Molnar, Human tooth wear, tooth function and cultural variability. *Am. J. Phys. Anthropol.* **34**, 175–189 (1971). Medline doi:10.1002/ajpa.1330340204

20. R. E. Green, A. S. Malaspinas, J. Krause, A. W. Briggs, P. L. Johnson, C. Uhler, M. Meyer, J. M. Good, T. Maricic, U. Stenzel, K. Prüfer, M. Siebauer, H. A. Burbano, M. Ronan, J. M. Rothberg, M. Egholm, P. Rudan, D. Brajković, Z. Kućan, I. Gusić, M. Wikström, L. Laakkonen, J. Kelso, M. Slatkin, S. Pääbo, A complete Neandertal mitochondrial genome sequence determined by high-throughput sequencing. *Cell* **134**, 416–426 (2008). Medline doi:10.1016/j.cell.2008.06.021

21. A. W. Briggs, U. Stenzel, P. L. Johnson, R. E. Green, J. Kelso, K. Prüfer, M. Meyer, J. Krause, M. T. Ronan, M. Lachmann, S. Pääbo, Patterns of damage in genomic DNA sequences from a Neandertal. *Proc. Natl. Acad. Sci. U.S.A.* **104**, 14616–14621 (2007). Medline doi:10.1073/pnas.0704665104

22. S. Sawyer, J. Krause, K. Guschanski, V. Savolainen, S. Pääbo, Temporal patterns of nucleotide misincorporations and DNA fragmentation in ancient DNA. *PLOS ONE* **7**, e34131 (2012). Medline doi:10.1371/journal.pone.0034131

23. J. Krause, A. W. Briggs, M. Kircher, T. Maricic, N. Zwyns, A. Derevianko, S. Pääbo, A complete mtDNA genome of an early modern human from Kostenki, Russia. *Curr. Biol.* **20**, 231–236 (2010). Medline doi:10.1016/j.cub.2009.11.068

24. J. Krause, Q. Fu, J. M. Good, B. Viola, M. V. Shunkov, A. P. Derevianko, S. Pääbo, The complete mitochondrial DNA genome of an unknown hominin from southern Siberia. *Nature* **464**, 894–897 (2010). Medline doi:10.1038/nature08976

25. Q. Fu, A. Mittnik, P. L. Johnson, K. Bos, M. Lari, R. Bollongino, C. Sun, L. Giemsch, R. Schmitz, J. Burger, A. M. Ronchitelli, F. Martini, R. G. Cremonesi, J. Svoboda, P. Bauer, D. Caramelli, S. Castellano, D. Reich, S. Pääbo, J. Krause, A revised timescale for human evolution based on ancient mitochondrial genomes. *Curr. Biol.* **23**, 553–559 (2013). Medline doi:10.1016/j.cub.2013.02.044

26. Q. Fu, H. Li, P. Moorjani, F. Jay, S. M. Slepchenko, A. A. Bondarev, P. L. Johnson, A. Aximu-Petri, K. Prüfer, C. de Filippo, M. Meyer, N. Zwyns, D. C. Salazar-García, Y. V.

Kuzmin, S. G. Keates, P. A. Kosintsev, D. I. Razhev, M. P. Richards, N. V. Peristov, M. Lachmann, K. Douka, T. F. Higham, M. Slatkin, J. J. Hublin, D. Reich, J. Kelso, T. B. Viola, S. Pääbo, Genome sequence of a 45,000-year-old modern human from western Siberia. *Nature* **514**, 445–449 (2014). Medline doi:10.1038/nature13810

27. P. Soares, L. Ermini, N. Thomson, M. Mormina, T. Rito, A. Röhl, A. Salas, S. Oppenheimer, V. Macaulay, M. B. Richards, Correcting for purifying selection: An improved human mitochondrial molecular clock. *Am. J. Hum. Genet.* **84**, 740–759 (2009). Medline doi:10.1016/j.ajhg.2009.05.001

28. I. Lazaridis, N. Patterson, A. Mittnik, G. Renaud, S. Mallick, K. Kirsanow, P. H. Sudmant, J. G. Schraiber, S. Castellano, M. Lipson, B. Berger, C. Economou, R. Bollongino, Q. Fu, K. I. Bos, S. Nordenfelt, H. Li, C. de Filippo, K. Prüfer, S. Sawyer, C. Posth, W. Haak, F. Hallgren, E. Fornander, N. Rohland, D. Delsate, M. Francken, J. M. Guinet, J. Wahl, G. Ayodo, H. A. Babiker, G. Bailliet, E. Balanovska, O. Balanovsky, R. Barrantes, G. Bedoya, H. Ben-Ami, J. Bene, F. Berrada, C. M. Bravi, F. Brisighelli, G. B. Busby, F. Cali, M. Churnosov, D. E. Cole, D. Corach, L. Damba, G. van Driem, S. Dryomov, J. M. Dugoujon, S. A. Fedorova, I. Gallego Romero, M. Gubina, M. Hammer, B. M. Henn, T. Hervig, U. Hodoglugil, A. R. Jha, S. Karachanak-Yankova, R. Khusainova, E. Khusnutdinova, R. Kittles, T. Kivisild, W. Klitz, V. Kučinskas, A. Kushniarevich, L. Laredj, S. Litvinov, T. Loukidis, R. W. Mahley, B. Melegh, E. Metspalu, J. Molina, J. Mountain, K. Näkkäläjärvi, D. Nesheva, T. Nyambo, L. Osipova, J. Parik, F. Platonov, O. Posukh, V. Romano, F. Rothhammer, I. Rudan, R. Ruizbakiev, H. Sahakyan, A. Sajantila, A. Salas, E. B. Starikovskaya, A. Tarekegn, D. Toncheva, S. Turdikulova, I. Uktveryte, O. Utevska, R. Vasquez, M. Villena, M. Voevoda, C. A. Winkler, L. Yepiskoposyan, P. Zalloua, T. Zemunik, A. Cooper, C. Capelli, M. G. Thomas, A. Ruiz-Linares, S. A. Tishkoff, L. Singh, K. Thangaraj, R. Villems, D. Comas, R. Sukernik, M. Metspalu, M. Meyer, E. E. Eichler, J. Burger, M. Slatkin, S. Pääbo, J. Kelso, D. Reich, J. Krause, Ancient human genomes suggest three ancestral populations for present-day Europeans. *Nature* **513**, 409–413 (2014). Medline doi:10.1038/nature13673

29. P. J. Reimer *et al*., IntCal13 and Marine13 Radiocarbon Age Calibration Curves 0–50,000 Years cal BP. *Radiocarbon* **55**, 1869–1887 (2013). doi:10.2458/azu_js_rc.55.16947

30. T. Higham, T. Compton, C. Stringer, R. Jacobi, B. Shapiro, E. Trinkaus, B. Chandler, F. Gröning, C. Collins, S. Hillson, P. O'Higgins, C. FitzGerald, M. Fagan, The earliest evidence for anatomically modern humans in northwestern Europe. *Nature* **479**, 521–524 (2011). Medline doi:10.1038/nature10484

31. M. White, P. Pettitt, Ancient digs and modern myths: The age and context of the Kent's Cavern 4 maxilla and the earliest *Homo sapiens* specimens in Europe. *Eur. J. Archaeol.* **15**, 392–420 (2012). doi:10.1179/1461957112Y.0000000019

32. W. E. Banks, F. d'Errico, J. Zilhão, Human-climate interaction during the Early Upper Paleolithic: Testing the hypothesis of an adaptive shift between the Proto-Aurignacian and the Early Aurignacian. *J. Hum. Evol.* **64**, 39–55 (2013). Medline doi:10.1016/j.jhevol.2012.10.001

33. A. Ronchitelli, S. Benazzi, P. Boscato, K. Douka, A. Moroni, Comments on "human-climate interaction during the Early Upper Paleolithic: Testing the hypothesis of an adaptive shift

between the Proto-Aurignacian and the Early Aurignacian” by William E. Banks, Francesco d’Errico, João Zilhão. *J. Hum. Evol.* **73**, 107–111 (2014). Medline doi:10.1016/j.jhevol.2013.12.010

34. C. Bronk Ramsey, S. Lee, Recent and planned developments of the program OxCal. *Radiocarbon* **55**, 720–730 (2013). doi:10.2458/azu_js_rc.55.16215
35. D. Fleitmann, H. Cheng, S. Badertscher, R. L. Edwards, M. Mudelsee, O. M. Göktürk, A. Fankhauser, R. Pickering, C. C. Raible, A. Matter, J. Kramers, O. Tüysüz, Timing and climatic impact of Greenland interstadials recorded in stalagmites from northern Turkey. *Geophys. Res. Lett.* **36**, L19707 (2009). doi:10.1029/2009GL040050
36. S. E. Bailey, J.-J. Hublin, Dental remains from the Grotte du Renne at Arcy-sur-Cure (Yonne). *J. Hum. Evol.* **50**, 485–508 (2006). Medline doi:10.1016/j.jhevol.2005.11.008
37. D. Panetta, N. Belcari, A. Del Guerra, A. Bartolomei, P. A. Salvadori, Analysis of image sharpness reproducibility on a novel engineered micro-CT scanner with variable geometry and embedded recalibration software. *Phys. Med.* **28**, 166–173 (2012). Medline doi:10.1016/j.ejmp.2011.03.006
38. L. A. Feldkamp, L. C. Davis, J. W. Kress, Practical cone-beam algorithm. *J. Opt. Soc. Am. A* **1**, 612–619 (1984). doi:10.1364/JOSAA.1.000612
39. P. S. Ungar, K. J. Fennell, K. Gordon, E. Trinkaus, Neandertal incisor beveling. *J. Hum. Evol.* **32**, 407–421 (1997). Medline doi:10.1006/jhev.1996.0109
40. P. J. Besl, N. D. McKay, A method for registration of 3D shapes. *PAMI* **14**, 239–256 (1992). doi:10.1109/34.121791
41. J. Dabney, M. Knapp, I. Glocke, M. T. Gansauge, A. Weihmann, B. Nickel, C. Valdiosera, N. García, S. Pääbo, J. L. Arsuaga, M. Meyer, Complete mitochondrial genome sequence of a Middle Pleistocene cave bear reconstructed from ultrashort DNA fragments. *Proc. Natl. Acad. Sci. U.S.A.* **110**, 15758–15763 (2013). Medline doi:10.1073/pnas.1314445110
42. M.-T. Gansauge, M. Meyer, Single-stranded DNA library preparation for the sequencing of ancient or damaged DNA. *Nat. Protoc.* **8**, 737–748 (2013). Medline doi:10.1038/nprot.2013.038
43. A. W. Briggs, U. Stenzel, M. Meyer, J. Krause, M. Kircher, S. Pääbo, Removal of deaminated cytosines and detection of in vivo methylation in ancient DNA. *Nucleic Acids Res.* **38**, e87 (2010). Medline doi:10.1093/nar/gkp1163
44. M. Meyer, M. Kircher, M. T. Gansauge, H. Li, F. Racimo, S. Mallick, J. G. Schraiber, F. Jay, K. Prüfer, C. de Filippo, P. H. Sudmant, C. Alkan, Q. Fu, R. Do, N. Rohland, A. Tandon, M. Siebauer, R. E. Green, K. Bryc, A. W. Briggs, U. Stenzel, J. Dabney, J. Shendure, J. Kitzman, M. F. Hammer, M. V. Shunkov, A. P. Derevianko, N. Patterson, A. M. Andrés, E. E. Eichler, M. Slatkin, D. Reich, J. Kelso, S. Pääbo, A high-coverage genome sequence from an archaic Denisovan individual. *Science* **338**, 222–226 (2012). Medline doi:10.1126/science.1224344
45. M. Meyer, M. Kircher, Illumina sequencing library preparation for highly multiplexed target capture and sequencing. *Cold Spring Harb Protoc*. **2010** (6): pdb.prot5448 (2010).

46. M. Kircher, S. Sawyer, M. Meyer, Double indexing overcomes inaccuracies in multiplex sequencing on the Illumina platform. *Nucleic Acids Res.* **40**, e3 (2012). Medline doi:10.1093/nar/gkr771

47. J. Dabney, M. Meyer, Length and GC-biases during sequencing library amplification: A comparison of various polymerase-buffer systems with ancient and modern DNA sequencing libraries. *Biotechniques* **52**, 87–94 (2012). Medline doi:10.2144/000113809

48. T. Maricic, M. Whitten, S. Pääbo, Multiplexed DNA sequence capture of mitochondrial genomes using PCR products. *PLOS ONE* **5**, e14004 (2010). Medline doi:10.1371/journal.pone.0014004

49. Q. Fu, M. Meyer, X. Gao, U. Stenzel, H. A. Burbano, J. Kelso, S. Pääbo, DNA analysis of an early modern human from Tianyuan Cave, China. *Proc. Natl. Acad. Sci. U.S.A.* **110**, 2223–2227 (2013). Medline doi:10.1073/pnas.1221359110

50. M. Kircher, U. Stenzel, J. Kelso, Improved base calling for the Illumina Genome Analyzer using machine learning strategies. *Genome Biol.* **10**, R83 (2009). Medline doi:10.1186/gb-2009-10-8-r83

51. G. Renaud, U. Stenzel, J. Kelso, leeHom: Adaptor trimming and merging for Illumina sequencing reads. *Nucleic Acids Res.* **42**, e141 (2014). Medline doi:10.1093/nar/gku699

52. H. Li, R. Durbin, Fast and accurate long-read alignment with Burrows-Wheeler transform. *Bioinformatics* **26**, 589–595 (2010). Medline doi:10.1093/bioinformatics/btp698

53. M. Ingman, H. Kaessmann, S. Pääbo, U. Gyllensten, Mitochondrial genome variation and the origin of modern humans. *Nature* **408**, 708–713 (2000). Medline doi:10.1038/35047064

54. A. W. Briggs, J. M. Good, R. E. Green, J. Krause, T. Maricic, U. Stenzel, C. Lalueza-Fox, P. Rudan, D. Brajkovic, Z. Kucan, I. Gusic, R. Schmitz, V. B. Doronichev, L. V. Golovanova, M. de la Rasilla, J. Fortea, A. Rosas, S. Pääbo, Targeted retrieval and analysis of five Neandertal mtDNA genomes. *Science* **325**, 318–321 (2009). Medline doi:10.1126/science.1174462

55. M. Meyer, Q. Fu, A. Aximu-Petri, I. Glocke, B. Nickel, J. L. Arsuaga, I. Martínez, A. Gracia, J. M. de Castro, E. Carbonell, S. Pääbo, A mitochondrial genome sequence of a hominin from Sima de los Huesos. *Nature* **505**, 403–406 (2014). Medline doi:10.1038/nature12788

56. K. Prüfer, F. Racimo, N. Patterson, F. Jay, S. Sankararaman, S. Sawyer, A. Heinze, G. Renaud, P. H. Sudmant, C. de Filippo, H. Li, S. Mallick, M. Dannemann, Q. Fu, M. Kircher, M. Kuhlwilm, M. Lachmann, M. Meyer, M. Ongyerth, M. Siebauer, C. Theunert, A. Tandon, P. Moorjani, J. Pickrell, J. C. Mullikin, S. H. Vohr, R. E. Green, I. Hellmann, P. L. Johnson, H. Blanche, H. Cann, J. O. Kitzman, J. Shendure, E. E. Eichler, E. S. Lein, T. E. Bakken, L. V. Golovanova, V. B. Doronichev, M. V. Shunkov, A. P. Derevianko, B. Viola, M. Slatkin, D. Reich, J. Kelso, S. Pääbo, The complete genome sequence of a Neanderthal from the Altai Mountains. *Nature* **505**, 43–49 (2014). Medline doi:10.1038/nature12886

57. M.-T. Gansauge, M. Meyer, Selective enrichment of damaged DNA molecules for ancient genome sequencing. *Genome Res.* **24**, 1543–1549 (2014). Medline doi:10.1101/gr.174201.114

58. P. Skoglund, B. H. Northoff, M. V. Shunkov, A. P. Derevianko, S. Pääbo, J. Krause, M. Jakobsson, Separating endogenous ancient DNA from modern day contamination in a Siberian Neandertal. *Proc. Natl. Acad. Sci. U.S.A.* **111**, 2229–2234 (2014). Medline doi:10.1073/pnas.1318934111

59. D. Reich, R. E. Green, M. Kircher, J. Krause, N. Patterson, E. Y. Durand, B. Viola, A. W. Briggs, U. Stenzel, P. L. Johnson, T. Maricic, J. M. Good, T. Marques-Bonet, C. Alkan, Q. Fu, S. Mallick, H. Li, M. Meyer, E. E. Eichler, M. Stoneking, M. Richards, S. Talamo, M. V. Shunkov, A. P. Derevianko, J. J. Hublin, J. Kelso, M. Slatkin, S. Pääbo, Genetic history of an archaic hominin group from Denisova Cave in Siberia. *Nature* **468**, 1053–1060 (2010). Medline doi:10.1038/nature09710

60. S. Horai, K. Hayasaka, R. Kondo, K. Tsugane, N. Takahata, Recent African origin of modern humans revealed by complete sequences of hominoid mitochondrial DNAs. *Proc. Natl. Acad. Sci. U.S.A.* **92**, 532–536 (1995). Medline doi:10.1073/pnas.92.2.532

61. K. Katoh, D. M. Standley, MAFFT multiple sequence alignment software version 7: Improvements in performance and usability. *Mol. Biol. Evol.* **30**, 772–780 (2013). Medline doi:10.1093/molbev/mst010

62. K. Tamura, G. Stecher, D. Peterson, A. Filipski, S. Kumar, MEGA6: Molecular Evolutionary Genetics Analysis version 6.0. *Mol. Biol. Evol.* **30**, 2725–2729 (2013). Medline doi:10.1093/molbev/mst197

63. A. Kloss-Brandstätter, D. Pacher, S. Schönherr, H. Weissensteiner, R. Binna, G. Specht, F. Kronenberg, HaploGrep: A fast and reliable algorithm for automatic classification of mitochondrial DNA haplogroups. *Hum. Mutat.* **32**, 25–32 (2011). Medline doi:10.1002/humu.21382

64. M. van Oven, M. Kayser, Updated comprehensive phylogenetic tree of global human mitochondrial DNA variation. *Hum. Mutat.* **30**, E386–E394 (2009). Medline doi:10.1002/humu.20921

65. A. J. Drummond, A. Rambaut, BEAST: Bayesian evolutionary analysis by sampling trees. *BMC Evol. Biol.* **7**, 214 (2007). Medline doi:10.1186/1471-2148-7-214

66. D. Posada, K. A. Crandall, MODELTEST: Testing the model of DNA substitution. *Bioinformatics* **14**, 817–818 (1998). Medline doi:10.1093/bioinformatics/14.9.817

67. S. Talamo, M. Richards, A comparison of bone pretreatment methods for AMS dating of samples >30, 000 BP. *Radiocarbon* **53**, 443–449 (2011).

68. R. Longin, New method of collagen extraction for radiocarbon dating. *Nature* **230**, 241–242 (1971). Medline doi:10.1038/230241a0

69. T. A. Brown, D. E. Nelson, J. S. Vogel, J. R. Southon, Improved Collagen Extraction by modified Longin method. *Radiocarbon* **30**, 171–177 (1988).

70. F. Brock, C. B. Ramsey, T. Higham, Quality assurance of ultrafiltered bone dating. *Radiocarbon* **49**, 187–192 (2007).

71. S. H. Ambrose, Preparation and characterization of bone and tooth collagen for isotopic analysis. *J. Archaeol. Sci.* **17**, 431–451 (1990). doi:10.1016/0305-4403(90)90007-R

72. G. J. van Klinken, Bone collagen quality indicators for palaeodietary and radiocarbon measurements. *J. Archaeol. Sci.* **26**, 687–695 (1999). doi:10.1006/jasc.1998.0385

73. B. Kromer, S. Lindauer, H.-A. Synal, L. Wacker, MAMS – A new AMS facility at the Curt-Engelhorn-Centre for Achaeometry, Mannheim, Germany. *Nucl. Instrum. Meth. B* **294**, 11–13 (2013). doi:10.1016/j.nimb.2012.01.015

74. K. K. Andersen, A. Svensson, S. J. Johnsen, S. O. Rasmussen, M. Bigler, R. Röthlisberger, U. Ruth, M.-L. Siggaard-Andersen, J. Peder Steffensen, D. Dahl-Jensen, The Greenland Ice Core Chronology 2005, 15–42 ka. Part 1: Constructing the time scale. *Quat. Sci. Rev.* **25**, 3246–3257 (2006). doi:10.1016/j.quascirev.2006.08.002

75. A. Svensson, K. K. Andersen, M. Bigler, H. B. Clausen, D. Dahl-Jensen, S. M. Davies, S. J. Johnsen, R. Muscheler, S. O. Rasmussen, R. Röthlisberger, The Greenland Ice Core Chronology 2005, 15–42 ka. Part 2: Comparison to other records. *Quat. Sci. Rev.* **25**, 3258–3267 (2006). doi:10.1016/j.quascirev.2006.08.003

76. A. Del Lucchese, F. Negrino, S. Simone, G. Vicino, in *Un siècle de construction du discours scientifique en Préhistoire* (26° Congrès Préhistorique de France, Avignon–Bonnieux 21-25, 2004), pp. 177–184.

77. M. Mussi, J. Cinq-Mars, P. Bolduc, Echoes from the mammoth steppe: The case of the Balzi Rossi. *Anal. Praehist. Leid* **31**, 105–124 (1999).

78. G. Vicino, Incisioni rupestri paleolitiche ai Balzi Rossi. *Riv. Ing. Int.* **26**, 51–56 (1971).

79. G. Vicino, Incisioni rupestri paleolitiche ai Balzi Rossi. *Riv. St. Lig.* **38**, 5–26 (1972).

80. G. Vicino, M. Mussi, Arte parietale ai Balzi Rossi: La Grotticella Blanc-Cardini (Ventimiglia, IM). *Origini* **23**, 21–38 (2011).

81. M. A. de Lumley, L'os iliaque anténéanderthalien de la grotte du Prince (Grimaldi, Ligurie italienne). *Bull. Mus. Anthropol. Préhist. Monaco* **18**, 89-112 (1972).

82. G. Vicino, Gli scavi preistorici nell'area dell'ex Casinò dei Balzi Rossi (Nota preliminare). *Riv. Ing. Int.* **27**, 77–97 (1972).

83. G. Vicino, La spiaggia tirreniana dei Balzi Rossi nei recenti scavi della zona dell'ex-casinò. *Atti della XVI Riunione Scientifica, Istituto Italiano di Preistoria e Protostoria, Firenze*, 75-95 (1974).

84. M. Cremaschi, A. Del Lucchese, F. Negrino, C. Ottomano, B. Wilkens, Ventimiglia (Imperia). Località Balzi Rossi. Nuovi dati sulla successione stratigrafica del ciclo interglaciale-glaciale-postglaciale. Scavi 1990. *Bollettino di Archeologia* **8**, 47–50 (1991).

85. A. Bietti, F. Negrino, in *New Approaches to the Study of Early Upper Palaeolithic "Transitional" Industries in Western Eurasia. Transitions Great and Small*, J. Riel-Salvatore, G. A. Clark, Eds. (B.A.R., Oxford, 2007), pp. 41–60.

86. A. Bietti, F. Negrino, L'Aurignacien et le Gravettien du Riparo Mochi, l'Aurignacien du Riparo Bombrini: Comparaisons et nouvelles perspectives. *Arch. Inst. Pal. Hum.* **39**, 133–140 (2008).

87. A. Bietti, A. Del Lucchese, F. Negrino, Nuovi studi e ricerche al Riparo Mochi (Balzi Rossi, Ventimiglia, Imperia). *Paleo-express* **7**, 4–6 (2001).

88. A. Bietti, A. Del Lucchese, F. Negrino, E. Spinapolice, in *Archeologia in Liguria, Nuova Serie, I, 2004-2005,* A. Del Lucchese, L. Gambaro, Eds. (Soprintendenza per i Beni Archeologici della Liguria, Genova, 2008), pp. 237-238.

89. A. Tagliacozzo, F. Zeppieri, I. Fiore, E. Spinapolice, A. Del Lucchese, Archaeozoological evidence of subsistence strategies during the Gravettian at Riparo Mochi (Balzi Rossi, Ventimiglia, Imperia - Italy). *Quat. Int.* **252**, 142–154 (2012). doi:10.1016/j.quaint.2011.03.059

90. C. Tozzi, F. Negrino, Nouvelles données sur les cultures moustériennes des grottes de Grimaldi. *Arch. Inst. Pal. Hum.* **39**, 101–107 (2008).

91. V. Formicola, P. B. Pettitt, A. Del Lucchese, A direct AMS radiocarbon date on the Barma Grande 6 Upper Paleolithic skeleton. *Curr. Anthropol.* **45**, 114–118 (2004). doi:10.1086/381008

92. V. Formicola, B. Holt, I resti umani del Paleolitico superiore della Liguria Occidentale: Una sintesi sui risultati degli studi recenti. *Bull. Mus. Anthropol. Préhist. Monaco*, **suppl. 1**, 96-102 (2008).

93. B. M. Holt, V. Formicola, Hunters of the Ice Age: The biology of Upper Paleolithic people. *Am. J. Phys. Anthropol.* **137** (Suppl 47), 70–99 (2008). Medline doi:10.1002/ajpa.20950

94. É. Rivière, De l'antiquité de l'homme dans les Alpes-Maritimes (Paris, 1887).

95. L. Cardini, Recenti scavi dell'Istituto Italiano di Paleontologia Umana alla Barma Grande di Grimaldi. *Arch. Antr. Etn.* **68**, 385–389 (1938).

96. G. Vicino, Lo scavo paleolitico al Riparo Bombrini (Balzi Rossi di Grimaldi, Ventimiglia). *Riv. Ing. Int.* **39**, 1–10 (1984).

97. V. Formicola, Un incisivo umano deciduo dal deposito aurignaziano del Riparo Bombrini ai Balzi Rossi. *Riv. Ing. Int.* **39**, 11–12 (1984).

98. D. Arobba, R. Caramiello, Analisi paleobotanica sui sedimenti del riparo Bombrini (Balzi Rossi, Ventimiglia). *Bull. Mus. Anthropol. Préhist. Monaco* **49**, 41-48 (2009).

99. S. Bertola *et al.*, La diffusione del primo Aurignaziano a sud dell'Arco alpino. *Preistoria Alpina* **47**, 17–30 (2013).

100. A. Del Lucchese, V. Formicola, B. Holt, F. Negrino, G. Vicino, Riparo Bombrini, Balzi Rossi (Ventimiglia, Imperia). Notizie preliminari degli scavi 2002-2004. *Ligures* **2**, 287–289 (2004).

101. F. Negrino, Riparo Bombrini, Balzi Rossi (Ventimiglia, IM): La campagna 2005. *Ligures* **3**, 194–196 (2005).

102. F. Negrino, C. Tozzi, Il Paleolitico in Liguria. *Bull. Mus. Anthropol. Préhist. Monaco* **suppl. 1**, 21-28 (2008).

103. J. Riel-Salvatore, I. C. Ludeke, F. Negrino, B. M. Holt, A spatial analysis of the Late Mousterian levels of Riparo Bombrini (Balzi Rossi, Italy). *Can. J. Archaeol.* **37**, 70–92 (2013).

104. S. Bertola, Approccio micropaleontologico discriminante per riconoscere la provenienza alpina o appenninica delle selci della scaglia rossa (Italia centro-settentrionale). *Bull. Mus. Anthropol. Préhist. Monaco* **52**, 17–27 (2012).

105. F. Negrino, E. Starnini, in *Les Matières Premières Lithiques en Préhistoire* (Actes de la Table Ronde Internationale, Aurillac, France, 2003), pp. 235–243.

106. M. Martini, E. Sibilia, S. Croci, M. Cremaschi, Thermoluminescence (TL) dating of burnt flints: Problems, perspectives and some example of application. *J. Cult. Herit.* **2**, 179–190 (2001). doi:10.1016/S1296-2074(01)01126-8

107. M. Peresani, M. Cremaschi, F. Ferraro, C. Falguères, J.-J. Bahain, G. Gruppioni, E. Sibilia, G. Quarta, L. Calcagnile, J.-M. Dolo, Age of the final Middle Palaeolithic and Uluzzian levels at Fumane Cave, Northern Italy, using 14C, ESR, 234U/230Th and thermoluminescence methods. *J. Arch. Sci.* **35**, 2986–2996 (2008). doi:10.1016/j.jas.2008.06.013

108. P. F. Cassoli, A. Tagliacozzo, Considerazioni paleontologiche, paleoeconomiche e archeozoologiche sui macromammiferi e gli uccelli dei livelli del Pleistocene superiore del Riparo di Fumane (VR) (Scavi 1988-91). *Boll. Mus. Civ. Stor. Nat. Verona* **18**, 349–445 (1991).

109. M. Peresani, A new cultural frontier for the last Neanderthals: The Uluzzian in Northern Italy. *Curr. Anthropol.* **49**, 725–731 (2008). doi:10.1086/588540

110. C. A. Jéquier, M. Romandini, M. Peresani, Les retouchoirs en matières dures animales: Une comparaison entre Moustérien final et Uluzzien. *C. R. Palevol* **11**, 283–292 (2012). doi:10.1016/j.crpv.2011.12.001

111. M. Peresani, Fifty thousand years of flint knapping and tool shaping across the Mousterian and Uluzzian sequence of Fumane cave. *Quat. Int.* **247**, 125–150 (2012). doi:10.1016/j.quaint.2011.02.006

112. M. Peresani *et al*., Fire-places, frequentations and the environmental setting of the final Mousterian at Grotta di Fumane: A report from the 2006-2008 research. *Quartär.* **58**, 131–151 (2011).

113. M. Peresani, I. Fiore, M. Gala, M. Romandini, A. Tagliacozzo, Late Neandertals and the intentional removal of feathers as evidenced from bird bone taphonomy at Fumane Cave 44 ky B.P., Italy. *Proc. Natl. Acad. Sci. U.S.A.* **108**, 3888–3893 (2011). Medline doi:10.1073/pnas.1016212108

114. M. Peresani, L. Centi, E. Di Taranto, Blades, bladelets and flakes: a case of variability in tool design at the onset of the Middle – Upper Palaeolithic transition in Italy. *Comptes Rendus Palevol.* **12**, 211-221 (+corrigendum) (2013).

115. M. Romandini, N. Nannini, A. Tagliacozzo, M. Peresani, The ungulate assemblage from layer A9 at Grotta di Fumane, Italy: A zooarchaeological contribution to the reconstruction of Neanderthal ecology. *Quat. Int.* **337**, 11–27 (2014). doi:10.1016/j.quaint.2014.03.027

116. A. Broglio, L'estinzione dell'Uomo di Neandertal e la comparsa dell'Uomo moderno in Europa. Le evidenze della Grotta di Fumane nei Monti Lessini. *Atti Istituto Veneto SS.LL.AA* **45**, 1–44 (1997).

117. A. Broglio, F. Gurioli, in *La spiritualité. Etudes et Recherches Archéologiques 106*, M. Otte, Ed. (Université de Liège, Liège, 2004), pp. 97–102.

118. C. Peretto *et al*., Living-Floors and Structures From the Lower Palaeolithic to the Bronze Age. *Coll. Anthrop.* **28**, 63–88 (2004).

119. A. Broglio *et al*., in *Production Lamellaires Attribuèes à l'Aurignacien*, F. Le Brun-Ricalens, Ed. (Luxembourg, Musée National d'Histoire et d'Art, 2005), pp. 415–436.

120. A. Broglio, M. De Stefani, A. Tagliacozzo, F. Gurioli, A. Facciolo, in *Kostenki and the Early Upper Paleolithic of Eurasia: General Trends, Local Developments*, S. A. Vasil'ev *et al*., Eds. (Nestor-Historia Saint Petersburg, 2006), pp. 263–268.

121. A. Broglio, M. De Stefani, F. Gurioli, P. Pallecchi, G. Giachi, T. Higham, F. Brock, L'art aurignacien dans la décoration de la Grotte de Fumane. *Anthropologie* **113**, 753–761 (2009). doi:10.1016/j.anthro.2009.09.016

122. D. H. Ubelaker, *Human Skeletal Remains. Excavations, Analysis, Interpretation* (Aldine, Chicago, 1978).

123. S. J. AlQahtani, M. P. Hector, H. M. Liversidge, Brief communication: The London atlas of human tooth development and eruption. *Am. J. Phys. Anthropol.* **142**, 481–490 (2010). Medline doi:10.1002/ajpa.21258

124. P. Graziosi, I. Balzi Rossi, *Itinerari Liguri 2* (Istituto Internazionale di Studi Liguri, Bordighera, 1976).

125. I. Crevecoeur, P. Bayle, H. Rougier, B. Maureille, T. Higham, J. van der Plicht, N. De Clerck, P. Semal, The Spy VI child: A newly discovered Neandertal infant. *J. Hum. Evol.* **59**, 641–656 (2010). Medline doi:10.1016/j.jhevol.2010.07.022

126. E. Trinkaus, V. A. Ranov, S. Lauklin, Middle paleolithic human deciduous incisor from Khudji, Tajikistan. *J. Hum. Evol.* **38**, 575–584 (2000). Medline doi:10.1006/jhev.1999.0370

127. T. K. Black 3rd; T. K. III, Sexual dimorphism in the tooth-crown diameters of the deciduous teeth. *Am. J. Phys. Anthropol.* **48**, 77–82 (1978). Medline doi:10.1002/ajpa.1330480111